CANCER GENOMICS & PROTEOMICS *15*: 91-114 (2018)
doi:10.21873/cgp.20068

Characterization of Camptothecin-induced Genomic Changes in the Camptothecin-resistant T-ALL-derived Cell Line CPT-K5

EIGIL KJELDSEN[1], CHRISTINE J.F. NIELSEN[2], AMIT ROY[2*], CINZIA TESAURO[2], ANN-KATRINE JAKOBSEN[3], MAGNUS STOUGAARD[3] and BIRGITTA R. KNUDSEN[2]

[1]*Cancer Cytogenetics Section, HemoDiagnostic Laboratory, and*
[3]*Department of Pathology, Aarhus University Hospital, Aarhus, Denmark;*
[2]*Department of Molecular Biology and Genetics, C.F. Møllers Allé, Aarhus University, Aarhus, Denmark*

Abstract. *Acquisition of resistance to topoisomerase I (TOP1)-targeting camptothecin (CPT) derivatives is a major clinical problem. Little is known about the underlying chromosomal and genomic mechanisms. We characterized the CPT-K5 cell line expressing mutant CPT-resistant TOP1 and its parental T-cell derived acute lymphoblastic leukemia CPT-sensitive RPMI-8402 cell line by karyotyping and molecular genetic methods, including subtractive oligo-based array comparative genomic hybridization (soaCGH) analysis. Karyotyping revealed that CPT-K5 cells had acquired additional structural aberrations and a reduced modal chromosomal number compared to RPMI-8402. soaCGH analysis identified vast copy number alterations and >200 unbalanced DNA breakpoints distributed unevenly across the chromosomal complement in CPT-K5. In addition, the short tandem repeat alleles were found to be highly different between CPT-K5 and its parental cell line. We identified copy number alterations affecting genes important for maintaining genome integrity and reducing CPT-induced DNA damage. We show for the first time that short tandem repeats are targets for TOP1 cleavage, that can be differentially stimulated by CPT.*

This article is freely accessible online.

**Current address:* Department of Biotechnology, National Institute of Pharmaceutical Education & Research (NIPER), Hajipur, Vaishali, India.

Correspondence to: Dr. Eigil Kjeldsen, Cancer Cytogenetics Section, HemoDiagnostic Laboratory, Aarhus University Hospital, Tage-Hansens Gade 2, Ent. 4A, DK-8000 Aarhus C, Denmark. E-mail: Eigil.Kjeldsen@clin.au.dk

Key Words: CPT-K5, camptothecin resistance, karyotype, aCGH, genomic instability, short tandem repeat.

The camptothecin (CPT) derivatives, topotecan and irinotecan (SN-38 being the active metabolite), belong to an important group of drugs used for the treatment of many types of malignancies in advanced stages, including colorectal, ovarian, small cell lung cancer and acute leukemia (1-5). However, acquired resistance to these drugs greatly compromises their efficacy in clinical use (6).

The CPTs are highly selective inhibitors of the nuclear enzyme DNA topoisomerase I (TOP1) [reviewed in (7)]. TOP1 is an important monomeric enzyme that is required to release the torsional tension of DNA introduced during the DNA replication and transcription processes in normal cells [reviewed in (8)]. Moreover, it has been shown that, in addition to its DNA-relaxing activity, TOP1 also has independent kinase activity important for splicing of pre-mRNA (9). The enzyme exerts its relaxing activity by transiently cleaving and rejoining one strand of the DNA duplex. The CPTs are non-competitive, reversible TOP1 inhibitors that cause accumulation of TOP1-cleavage complexes (TOP1-cc) in the genome by transiently preventing the DNA rejoining step of catalysis. The trapped TOP1-cc are converted into one-ended DNA double-strand breaks (DSBs) when they collide with the DNA replication or transcription machinery. It is generally accepted that the formation and stabilization of TOP1-cc and their conversion into one-ended DSBs is a prerequisite for the cytotoxic activity of CPTs (10).

Although many players have been implicated in the cellular response to CPT, little is known about the pathways downstream of the trapped TOP1-cc that ultimately lead to repair of DNA damage or cell death. Impaired DSB repair makes cells hypersensitive to CPT and unless the DSBs are repaired they are lethal to the cell. DNA repair may lead to chromosomal or genomic alterations depending on the involved pathways. Several CPT-resistant cell lines have been derived (11-22), but only few of these have been characterized at the chromosomal or genomic level (21, 23).

In the present study we aimed to characterize the chromosomal complement and global copy number aberrations generated by acquired CPT resistance in the CPT-K5 cell line to gain insight into which regions of the genome may be affected in acquisition of CPT resistance. Furthermore, we examined whether short tandem repeat (STR) sequences, normally used for paternity testing and cell line authentication, are targets for TOP1 DNA cleavage, and whether these DNA cleavage sites can be selectively stimulated by CPT.

Materials and Methods

Cell lines and cell proliferation analysis. Andoh and co-workers established the CPT-resistant cell line, CPT-K5, from its parental sensitive counterpart human T-cell derived acute lymphoblastic (T-ALL) cell line RPMI-8402 (wild-type) by exposure to stepwise increasing concentrations of the semi-synthetic water-soluble CPT-derivative, irinotecan (11). For this study, cells stored in liquid nitrogen were thawed and cultured briefly at an initial density of 1×10^6 cells/ml in RPMI 1640 medium supplemented with 10% fetal calf serum as described elsewhere (24). Growth inhibition of the cells by CPT was determined by counting the number of cells in culture using a hematology analyzer (Sysmex KX-21N; Sysmex Nordic Aps, Copenhagen, Denmark).

Nuclear extracts, western blotting, and measurement of tyrosyl-DNA phosphodiesterase 1 (TDP1) and TOP1 activity. Preparation of nuclear extracts from RPMI-8402 and CPT-K5 cells, TOP1-specific western blotting and TOP1 activity measurements by rolling-circle enhanced enzyme activity detection (REEAD) was performed as described previously (25), while TDP1 activity measurement was performed as described in (26).

Expression and purification of recombinant human TOP1. Recombinant human TOP1 was expressed in yeast and purified to homogeneity, as described previously (27). The enzyme preparation was tested for purity by sodium dodecyl sulfate (SDS) polyacrylamide gel electrophoresis followed by Coomassie staining and the concentration estimated by comparison to a bovine serum albumin (BSA) standard before use.

G-Banding and fluorescence in situ hybridization (FISH). Chromosomal preparations and G-banding were performed according to standard protocols as described in (28). Karyotypes and FISH results were reported according to ISCN, 2013 (29). Analysis of 10 G-banded metaphases was carried out using a Laborlux microscope (Leica, Germany) equipped with a grey-level charge coupled device-camera and Ikaros karyotyping software implemented on a Dell Optiplex GX1 (MetaSystems, Heidelberg, Germany). Locus-specific FISH analysis of interphase nuclei and metaphase spreads was carried out with the following directly fluorescent labeled probe sets according to the manufacturers' instructions: SIL-TAL1 FISH DNA probes and TOP1/CEN20 (DAKO, Glostrup, Denmark); BlueFISH Bacterial Artificial Chromosomes (BAC) probes (BlueGnome, Cambridge, UK): RP11-133H19 fluorescence labeled with red (11p15.4, pos. 8,555,486-8,732,332 bp located telomeric to the LIM domain only 1 (*LMO1*) gene pos. 8,202,433-8,241,982) and RP11-298I3 (14q11.2, pos. 22,435,253-22,627,198 located centromeric to the Tcrd T cell receptor delta chain (*TCRD*) gene pos. 21,994,085-22,002,042); and custom-made BAC-based probes (Empire Genomics, Buffalo NY, USA): RP11-368G2 (4q22.1, pos. 89,137,575-89,319,451), and RP11-213O13 (14q32.11, pos. 89,466,687-89,648,208) were used for validation of array-based comparative genomic hybridization (aCGH) results. Interphase nuclei and metaphases were counterstained with 4',6-diamidino-2-phenylindole (DAPI). The genomic position of the listed BAC probes was according to National Center for Biotechnology Information (NCBI) build 36.1 (hg18) (http://www.ncbi.nlm.nih.gov).

Spectral karyotyping (SKY). Pretreatment, denaturing, and hybridization of microscopy slides with chromosome suspension applied were carried out as previously described (30) according to the manufacturer's instructions (Applied Spectral Imaging™, Migdal HaEmek, Israel). Ten fully analyzed mitoses in the SKY analysis were performed for both cell lines. Numerical and structural aberrations were counted using a normal female as reference. Karyotypes were described according to International System for Human Cytogenetic Nomenclature (ISCN) (29)

aCGH analysis. High-resolution aCGH analysis was performed using the 180k oligo-based Cancer CytoChip (BlueGnome) as described elsewhere (31). In brief, high molecular weight DNA was isolated from RPMI-8402 and CPT-K5 cells using Gentra Pure Gene kit (Qiagen AB, Sollentuna, Sweden) according to the manufacturer's instructions. Pooled female DNA (Promega, Biotech AB, Nacka, Sweden) was used as reference DNA to determine the DNA copy number status of the female RPMI-8402 cells and derivative CPT-K5 cells. In addition, subtractive aCGH analysis of CPT-K5 was performed with isolated DNA from the parental cell line RPMI-8402 as reference DNA. The analysis was carried out according to the manufacturer's instructions using 0.5 μg of DNA. After hybridization, washing and drying, the oligo arrays were scanned at 2.5 μm with a GenePix 4400A microarray scanner (Molecular Devices, Sunnyvale, CA, USA). Initial analysis and normalization was achieved with BlueFuseMulti v2.6 (BlueGnome). For analysis and visualization, log2 probe signal values were imported into Nexus Copy Number software v6.1 (BioDiscovery, Hawthorne, CA, USA), and segmented using RANK segmentation algorithm with a minimum of five probes/segment. Gains and losses were defined by log2 ratios 0.16 and −0.16, respectively, while 0.5 and −1.0 defined high copy gains and large losses, respectively. The reference genome was NCBI build 36.1 (hg18). Bioinformatics analysis was performed by querying the University of California, Santa Cruz database (http://genome.ucsc.edu).

Genomic break point analysis. Break points were defined with high precision as locations where a change in copy number occurred in called regions of amplifications and deletions as determined by the Nexus software algorithm. To quantify genomic breakage, $\log_2$ ratio differences larger than 0.3 were used to discriminate putative DNA breakage points. We identified those breakage points at the edges of segments of copy number gains and losses as well as points of abrupt copy number changes called within larger aberrations. The precision of this type of measurement is determined by the resolution of the array. The smallest aberration we were able to detect with confidence on the 180k platform was 100 kb in length. In addition, the abnormality needed to be present in at least 10-20% of the cells in order to be detected.

Immunophenotyping by flow cytometry. Immunophenotyping of exponentially growing RPMI-8402 and CPT-K5 cells were carried out as described in (32).

STR profiling. STR profiling was performed at the Department of Forensic Medicine, University of Copenhagen, Copenhagen, Denmark, as part of their routine analyses using the AmpFISTR® Identifiler PCR Amplification kit (Applied Biosystems, Thermo Fisher Scientific, Waltham, MA, USA). The STR profiling was repeated twice with identical results on genomic DNA purified from two independent cultures from both cell lines.

Generation of STR TOP1 cleavage substrates. The flanking sequences in the STR TOP1 cleavage substrates were the same in the three substrates (marked below in bold) and the STR repeat length (marked with underline) were from the parental CPT-sensitive 8402 cell line.

Each of the STR TOP1 cleavage substrates were synthesized as single-stranded oligonucleotides (DNA technology, Aarhus, Denmark).

I) D7S820 locus (8 repeats of GATA): 50-base top strand (5'->3'): **ACGTCACGG**GATAGATAGATAGATAGATAGATAGATAGATAGATA**CGGTTCAGC**; 50-base bottom strand (5'->3'): **GCTGAACCG**TATCTATCTATCTATCTATCTATCTATCTATC**CCGTGACGT**.

II) D5S818 locus (12 repeats of AGAT): 60-base top strand (5'->3'): **ACGTCACGG**AGATAGATAGATAGATAGATAGATAGATAGATAGATAGATAGATAGAT**CGGTTCAGC**; 60-base bottom strand (5'->3'): **GCTGAACCG**ATCTATCTATCTATCTATCTATCTATCTATCTATCTATCTATCTATCTATCT**CCGTGACGT**.

III) Thyroid peroxidase (*TPOX*) locus (8 repeats of AATG): 50-base top strand (5'->3'): **ACGTCACGG**AATGAATGAATGAATGAATGAATGAATGAATGAATG**CGGTTCAGC**; 50-base bottom strand (5'->3'): **GCTGAACCG**CATTCATTCATTCATTCATTCATT CATT CATTCATT**CCGTGACGT.**

To prepare the STR substrates for TOP1 cleavage reaction, 50 pmol of each top strand was separately hot-labeled with gamma-ATP essentially as described before (33). The reaction was stopped by ethanol precipitation using NaCl and after 80% EtOH wash, and drying of the pellet, it was resuspended in 10 µl 1x TOP1-cleavage buffer (5 mM $MgCl_2$, 5 mM $CaCl_2$, and 10 mM Tris-HCl, pH 7.5). Then 50 pmol of the corresponding bottom strand was added, the mixture was left at 90˚C for 2 min and allowed to anneal with the respective top strand by slowly cooling down to room temperature.

TOP1 STR cleavage reactions and detection. The TOP1 cleavage reaction was performed as described (33). Briefly, approximately 200 copies of the annealed oligonucleotides were used for cleavage reaction with 300 units of human TOP1 in the presence of 10 µM CPT or dimethylsulfoxide, which was used as a solvent for CPT. The reaction was carried out at 37˚C for 30 min. and stopped by the addition of 0.2% SDS followed by EtOH precipitation. After precipitation and 80% EtOH washing and drying of the pellet, it was resuspended in 10 µl trypsin mix and incubated at 37˚C for 30 min as described previously (33). Then 10 µl of 2x Seq-buffer (100% formamide, 1 mM EDTA, pH 8.0, 0.1% bromophenol blue (BPB), and 0.1% xylene cyanol) (Sigma-Aldrich, Brøndby, Denmark) was added to each reaction. Approximately 16 counts per second was added to each lane of a 14% denaturating polyacrylamide gel and run until BPB left the gel. The gel was transferred to Whatman 3MM filter paper (Sigma-Aldrich Chemie GmbH), dried and exposed in a phosphor imager (PMI Imager; Bio-Rad, Life Science, Bio-RAD laboratories, Copenhagen, Denmark).

Table I. *Immunophenotype of RPMI-8402 and CPT-K5.*

Antigen	RPMI-8402[a] (DMSZ)	RPMI-8402	CPT-K5
CD2	+	+	+
CD3	-	-	-
CD4	-	n.d.[c]	n.d
CD5	+	+	+
CD6	+	n.d.	n.d.
CD7	+	+	+
CD8	-	-	-
CD13	-	-	-
CD19	-	-	-
CD33	n.i.[b]	-	-
CD34	+	+	-
CD45	n.i.	+	+
CD71	n.i.	+	+
CD235a	n.i.	-	-
TCR–α/β	-	n.d.	n.d.
TCR-γ/δ	-	n.d.	n.d.

[a]Information from DMSZ web-site, http://www.dsmz.de; [b]n.i., no information; [c]n.d., not done.

Results and Discussion

Cellular characteristics of CPT-K5 and its CPT-resistant CPT-K5 cell line. To obtain a global genomic insight into the development of acquired CPT resistance and to identify putative candidate genes involved in this process, we took advantage of the CPT-K5 cell line, which exhibits highly stable CPT resistance following prolonged CPT-selective growth of its parental RPMI-8402 cell line (11, 24, 34).

For the purposes of the present study, we wanted to confirm the cellular and biochemical characteristics of these cell lines using current methods. Firstly, immunophenotyping of the parental cell line RPMI-8402 confirmed that it is indeed a T-ALL derived cell line (Table I). The CPT-K5 cell line has not previously been characterized by immunophenotyping but this analysis confirmed that CPT-K5 retains the predominant T-ALL immunophenotype (Table I). Secondly, at the genetic level it was confirmed that the RPMI-8402 harbors two T-ALL specific chromosomal aberrations: i) the common *SIL* deletion at chromosome region 1p32; and ii) the rare t(11;14)(p15;q11)/*LMO1-TCRD*. Both aberrations were present in two copies (Figure 1). CPT-K5 has retained one of the chromosome 1 that harbors the 1p32 deletion, while the t(11;14) was completely lost (Figure 1). Thirdly, in a standard cell survival assay the CPT-resistant and the CPT-sensitive phenotypes of the CPT-K5 and RPMI-

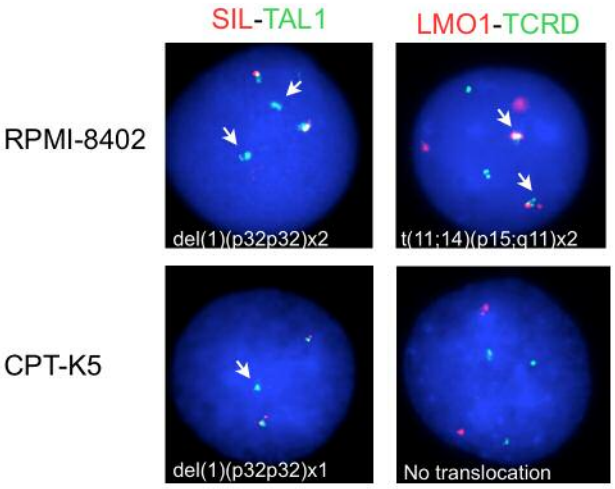

Figure 1. *Fluorescence in situ hybridization (FISH) analysis of RPMI-8402 cell line using the SIL-TAL1 split-apart probe set showing a nucleus with 2F2G pattern indicating deletion of the SCL/TAL1-Interrupring locus (STIL) gene in two alleles and a normal fusion in the other two alleles. FISH analysis using of RPMI-8402 cell line using the LMO1-TCRD single fusion probe showing a nucleus with 2F2R2G pattern indicating fusion of the LIM domain only 1 (LMO1) and the Tcrd T cell receptor delta chain (TCRD) genes in two alleles and no fusion in the other two alleles. FISH analysis of CPT-K5 cell line using the TAL1-STIL split-apart probe showing a nucleus with 2F1G pattern indicating deletion of the STIL gene in one allele and a normal fusion in the other two alleles. FISH analysis using of CPT-K5 cell line using the LMO1-TCRD single fusion probe showing a nucleus with 3R3G pattern indicating no fusion of the genes.*

8402 cell lines, respectively, were confirmed. As demonstrated in Figure 2A, cell proliferation was significantly reduced in the presence of 1 μM CPT in the CPT-sensitive parental cell line RPMI-8402, while the CPT-resistant derivative cell line, CPT-K5, did not exhibit any significant change in growth rate. In the absence of CPT, the cellular growth rate of the CPT-K5 was lower as compared to its parental cell line, which seems to be a common feature of CPT-resistant cell lines (22). Fourthly, we compared the TOP1 activity expressed in the two cell lines by western blotting and REEAD assay (35, 36). In line with previous studies, we found a reduced intra-cellular level of TOP1 protein in CPT-K5 cells relative to RPMI-8402 cells (Figure 2B). The cellular TOP1 activity was measured using the REEAD assay, which allows quantification of TOP1 cleavage-ligation activity in crude extracts from only a few human cells (schematically illustrated in Figure 2C) (35, 36). With the REEAD assay, we found a 2- to 3-fold reduction in cellular TOP1 enzymatic activity (Figure 2D). Moreover, the previously observed CPT-resistant phenotype of purified TOP1 expressed in CPT-K5 cells (11, 24) was confirmed by measuring the effect of CPT on TOP1 activity present in crude extracts from the CPT-K5 and its parental cell lines using the REEAD assay (Figure 2E).

Taken together, our present findings are in agreement with previous studies by Andoh *et al*. (11) and Kjeldsen *et al*. (24), and establish that the CPT-K5 cell line is a T-ALL derived cell line with unique characteristics.

Chromosomal analysis of CPT-K5 and RPMI-8402 cells. The CPT-K5 cell line has not previously been characterized by karyotyping, whereas its parental cell line RPMI-8402 had a partial or incomplete karyotype available as described elsewhere (37-40) and by DSMZ (Braunschweig, Germany; http://www.dsmz.de). In agreement with these earlier reports, we found that the RPMI-8402 cell line is hypo-tetraploid with a modal chromosomal number of 90 (range=76-92) (Figure 3A and B; Table II). In the present study, we completed the karyotype by defining the three previously assigned marker chromosomes to be: del(X)(q13.2q22.1), del(2)(q11.2q23.7) and der(15)t(14;15)(q32.2;p11).

The karyotype of the CPT-K5 cell line is also hypo-tetraploid but with a modal chromosome number of 80 (range=71-81) (Figure 3C and D; Table II). The most prominent differences between CPT-K5 and its parental RPMI-8402 are: i) a reduced modal chromosomal number from 90 to 80; ii) loss of five structurally aberrant chromosomes: del(Xq), del(2q), dup(4q), del(6q), and t(11;14); and iii) gain of 13 new structurally aberrant chromosomes: der(1)t(1;10), der(2)t(2;6), der(4)t(4;17), der(6)t(6;16), der(7)t(7;8), der(8)t(8;9), der(9)t(4;9), der(10)t(10;20), der(12)t(4;12), der(16)t(3;16), der(19)t(3;19), der(20)t(9;20), and der(22)t(3;22;3). Despite these major karyotypic differences between the two cell lines affecting almost all chromosomes, chromosomes 5, 18, and 21 were cytogenetically unaffected.

Although several human cell lines resistant to CPT or its derivatives have been developed (Table III) only the CPT-K5 cell line has so far been studied by karyotyping analysis as described above. This is intriguing from a biological point of view since TOP1 exerts its main activity in DNA metabolism by cleavage and rejoining, and that the latter is inhibited by CPT causing DNA strand breaks, which ultimately may induce chromosomal aberrations and genomic instability (23, 41). Spectral karyotyping of the doxorubicin-resistant cell line, NCI-H69AR, which is cross-resistant to several topoisomerase II inhibitors, revealed substantial structural chromosomal differences compared with its parental NCI-H69 cell line (42). Similar chromosomal findings were obtained for mitoxantrone-resistant SF295 cells (43). Together these data suggest that acquisition of resistance to drugs inhibiting DNA cleavage-rejoining/metabolizing topoisomerases is accompanied by major karyotypic alterations, although the molecular mechanisms behind such alterations remain obscure.

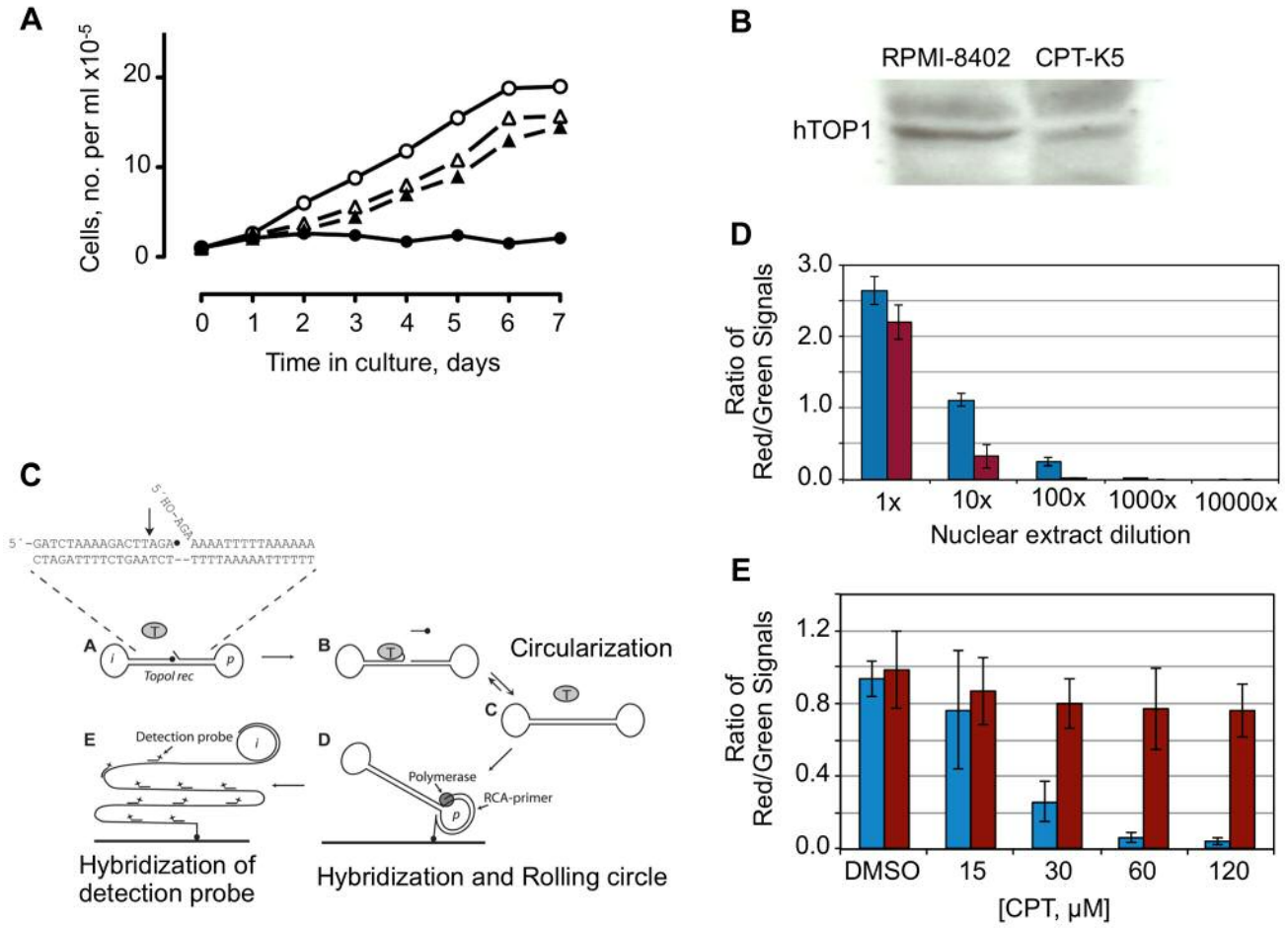

Figure 2. *A: Effects of camptothecin (CPT) on cell growth of parental RPMI-8402 and CPT-K5 cells. Growth of parental cells in the absence (○) and presence of 1 μM CPT (●). Growth of CPT-K5 in the absence (△) and presence of 1 μM CPT (▲). B: Western blot of nuclear extracts from 10^6 cells of RPMI-8402 and CPT-K5 using mouse antibody against human topoisomerase 1 (hTOP1). C: Schematic representation of the rolling-circle enhanced enzyme activity detection (REEAD) assay. A dumbbell-shaped DNA substrate with a preferred TOP1 cleavage sequence in the double-stranded stem region and an identifier- or primer annealing sequence (denoted "i" or "p") in each of the loops is converted to a closed circle upon cleavage and ligation by TOP1. The generated circle is then hybridized to a surface anchored primer with a sequence matching the "p" region and subjected to rolling circle amplification by added phi-polymerase. The resulting tandem repeat rolling circle product is visualized at the single molecule level by hybridization of fluorescent labeled detection probes matching the "i" region. D: REEAD measurement of hTOP1 in nuclear extracts generated from 106 cells and assayed either undiluted (1x) or 10, 100, 1000, or 10,000 times diluted as indicated. E: The CPT sensitivity of hTOP1 in extracts from RPMI-8402 (blue bars) and CPT-K5 (red bars) was analyzed by measuring the activity using the REEAD assay in the presence of increasing concentrations of CPT as indicated. The bar chart shows the mean values from three independent experiments and the error bars indicate standard deviations.*

Genomic profiling reveals greatly increased number of genomic DNA breakpoints in CPT-K5 cells. To further characterize the observed chromosomal differences between RPMI-8402 and CPT-K5 cells, we examined copy number changes between the cell lines by oligo-based aCGH analysis using female DNA pooled from normal individuals as reference (Figure 4A). For RPMI-8402 cells, the observed copy number aberrations were in agreement with the published SNP Array Based LOH and Copy Number Analysis (Welcome Sanger Trust Institute, http://www.sanger.ac.uk/cgi-bin/genetics/CGP/cghviewer). The oligo-based aCGH analysis of CPT-K5 cells confirmed the major differences as revealed by karyotyping (Figure 4B).

For a detailed comparison, however, the approach of comparing oaCGH analyses with DNA from normal individuals serving as a reference is imprecise. Subtractive CGH analysis is a direct method for determining genomic changes between drug-resistant cell lines where DNA from

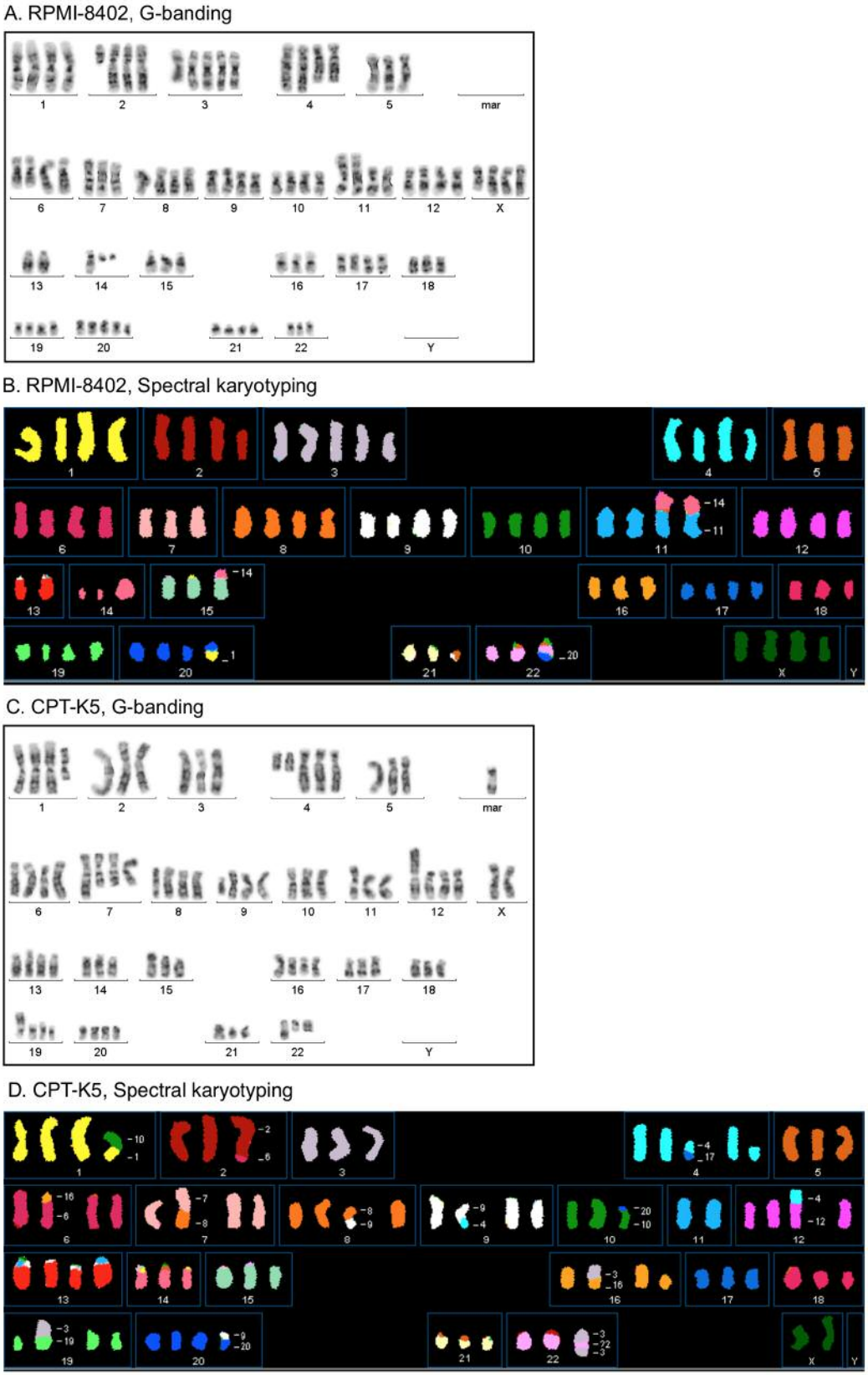

Figure 3. *G-Banding (A, C) and spectral karyotyping (B,D) of the RPMI-8402 (A,B) and CPT-K5 (C,D) cell lines showing representative karyotypes.*

Table II. *Karyotypes of the camptothecin (CPT)-resistant cell line CPT-K5 and its parental CPT-sensitive RPMI-8402 cell line.*

Cell line	Karyotype
RPMI-8402	90<4n>,XXX,del(X)(q13.2q22.1), del(2)(q11.2q37.3), +3, dup(4)(q13.1q25)x2, -5, del(6)(q13q21)x2, -7, t(11;14)(p15;q11)x2, -13, -13, -15, der(15)t(14;15)(q32.2;p11), -16, -18, der(20)t(1;20)(p36.1;q11.21), der(22)t(20;22)(q11.21;q13.33) and a minor sideline with an additional der(1)t(1;8)(p3?5;q11)
CPT-K5	80<4n>,XX,-X,-X,der(1)t(1;10)(p10;q11)del(1)(q25),-2,t(2;6)(q37::p12.3p11.2),-3,+4,der(4)t(4;17)(q?11;q25), del(4)(q11), -5, der(6)t(6;16)(p21;q11), der(7)t(7;8)(q36;q13), der(8)t(8;9)(q12;q33), i(9)(q10),der(9)t(4;9), -10, der(10)t(10;20)(p15;?), -11,-11, t(4;12)(q22q21::p13),-14,-15,der(16)t(3;16)(q21;q11),-17,-18, der(19)t(3;19)(p21;p13), der(20)t(9;20), -21, der(22)t(3;22;3) and a minor sideline with del(6)(q14q21)

Table III. *Human cell lines developed after selection of resistance to camptothecin (CPT) or its derivatives.*

Resistant cell line	Parental	Parental cancer	Selection agent	*TOP1* point mutation	Karyotype available (Ref)	Reference
CPT-K5	RPMI-8402	T-ALL	CPT-11	Asp533Gly	P: Yes (see Table II) R: Yes, present study (see Table II)	(11, 34)
PC-7/CPT	PC-7	Non-small cell lung cancer	CPT-11	Thr729Ala	P: No R: No	(12, 13)
A549/CPT	A549	Lung cancer	CPT	None	P: Yes, (97) R: No, but CGH analysis (44)	(14)
St-4/CPT	St-4	Gastric cancer	CPT	No, but ex3 to ex9 deletion	P: No R: No, but CGH analysis (44)	(14)
HT-29/CPT	HT-29	Colon cancer	CPT	No, but ex3 to ex9 deletion	P: No R: No, but CGH analysis, (44)	(14)
U937/CR	U937	Myeloid leukemia	9-NC	Phe361Ser	P: Yes (98) R: No	(15)
CEM/C1 and CEM/C2	CCRF-CEM	T-ALL	CPT*	Asn722Ser	P: Yes (99) R: No	(16)
DU-145/RC0.1 DU-145/RC1	DU145	Prostate cancer	9-NC	Arg364His	P: Yes (100, 101) R: No	(17, 18)
U937/RERC	U937	Myeloid leukemia	9-NC	Asp533Asn	P: Yes R: No	(19)
CPT30	HONE-1	Nasopharyngeal carcinoma	CPT	Glu418Lys	P: No R: No	(20)
MMRU/CR1 and MMRU/CR2	MMRU	Melanoma	CPT-11	None	P: No R: No, but BAC-based aCGH analysis (21)	(21)
SF295/hCPT50 and SF295/BN50	SF295	Glioblastoma	hCPT and BN80915	None	P: Yes (43) R: No	(55)
HT-29/SN-38	HT-29	Colon cancer	SN38	None	P: No	(22)
HCT-116/SN-38	HCT-116	Colon cancer		Arg364Lys and Gly721Arg	R: No	

P: Parental; R: resistant; T-ALL: T-cell lymphoblastic leukemia, 9-NC: 9-nitro-20(*S*)camptothecin; hCPT: homocamptothecin; BN80915: hCPT derivative; SN-38:7-ethyl-10-hydroxy-20(S)-camptothecin. *Resistance stable for up to 6 months.

the parental cell line serves as reference DNA (44, 45). The subtractive oligo-based aCGH analytical approach, where the RPMI-8402 DNA served as a reference, revealed that CPT-K5 cells had acquired 165 copy number alterations (Figure 4C, Table IV).

Calculating the mere number of copy number alterations underestimates the number of putative DNA breakage points (46). We assessed those DNA breakage points at the edges of segments of DNA copy number gains and losses, as well as at points of abrupt DNA copy number changes called within larger aberrations as exemplified in Figure 4D. By this analysis, we found that CPT-K5 cells had acquired a total of 236 unbalanced breakpoints that were unevenly distributed across each chromosome (Figure 4D). The

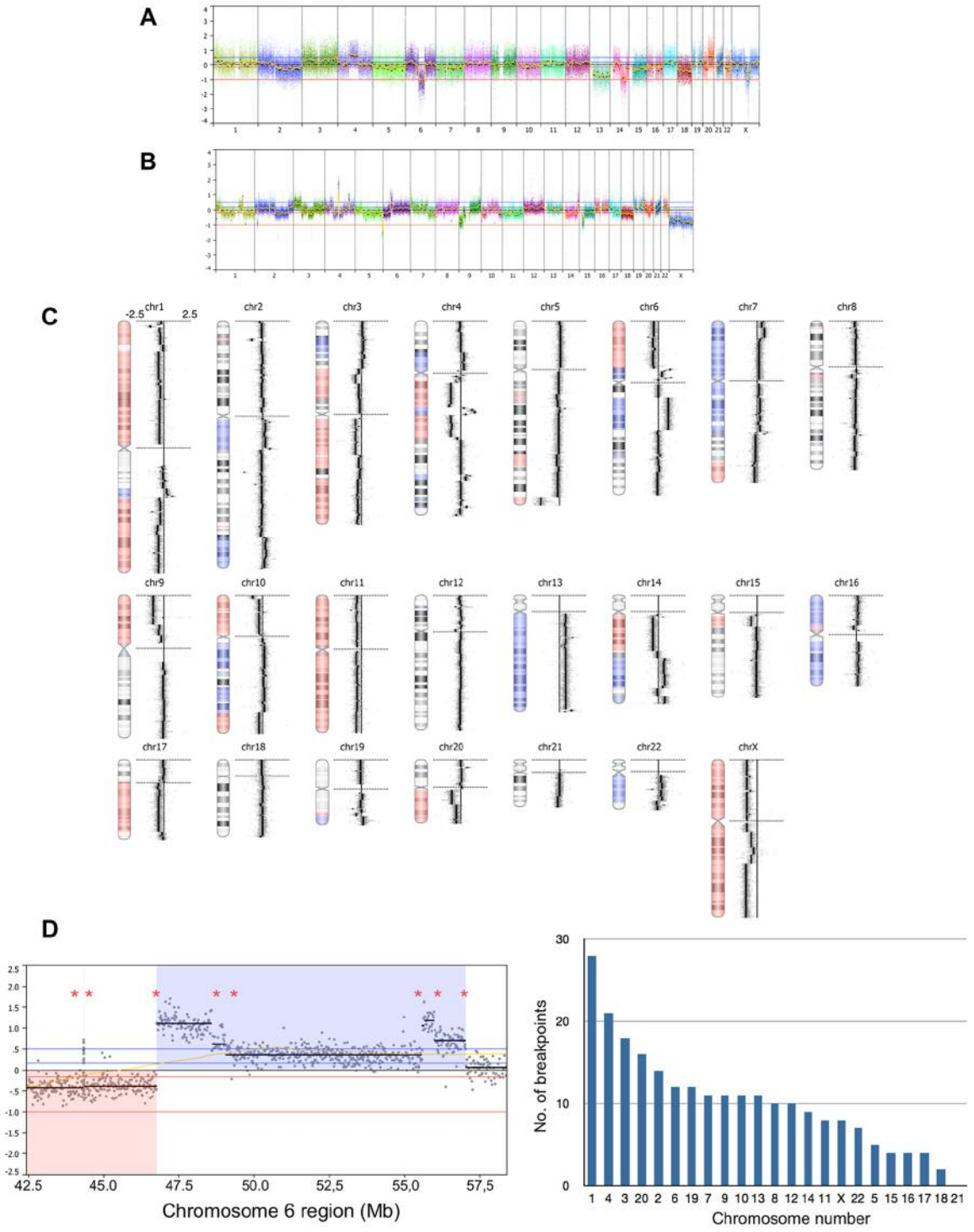

Figure 4. *Genomic profiling using 180k oligo-based array comparative genomic hybridization (aCGH) analysis. A: Whole-genome view of RPMI-8402 against normal female DNA pool. B: Whole-genome view of CPT-K5 against normal female DNA pool. C: Subtractive aCGH analysis where RPMI-8402 served as reference. To the right of the individual ideograms, microarray profiles of copy number gains and losses are depicted. Gain is indicated by blue and loss is indicated by red as an overlay on the ideogram. The log2 ratios for each chromosome are −2.5, 0, and +2.5 as illustrated for chromosome 1. D: Subtractive aCGH-based breakpoint analysis. Left panel: Magnified view of copy number profile of a region on chromosome 6 (pos. 42,500,000-58,000,000 bp) in which asterisks indicate determined putative DNA breakpoints. Focusing on the called regions of loss (red) and gain (blue) indicates two breakpoints, while taking copy number changes within the called regions into account, eight putative DNA break points can be determined. Right panel. Diagram showing the number of putative DNA break points determined on each chromosome.*

Table IV. *Results from subtractive oligo array-based comparative genomic hybridization analysis between CPT-K5 and RPMI-8402 (hg18) cell lines*.

Chromosomal region	Copy number aberration	Length (bp)	Cytoband	No. of probes
chr1:0-4,617,760	Loss	4617761	p36.33 - p36.32	347
chr1:4,617,760-6,731,626	Homozygous copy loss	2113867	p36.32 - p36.31	135
chr1:6,731,626-23,383,050	Loss	16651425	p36.31 - p36.12	1028
chr1:29,939,359-40,135,057	Loss	10195699	p35.3 - p34.2	667
chr1:40,232,695-47,470,334	Loss	7237640	p34.2 - p33	518
chr1:47,555,023-76,314,989	Loss	28759967	p33 - p31.1	1702
chr1:76,687,243-121,052,423	Loss	44365181	p31.1 - p11.2	2547
chr1:147,259,828-148,058,607	Loss	798780	q21.1 - q21.2	30
chr1:164,645,796-171,310,019	Gain	6664224	q24.1 - q25.1	417
chr1:171,310,019-172,363,398	High copy gain	1053380	q25.1	62
chr1:172,363,398-172,978,604	Gain	615207	q25.1	37
chr1:172,978,604-247,249,719	Loss	74271116	q25.1 - q44	4372
chr2:82,105-2,351,466	Loss	2269362	p25.3	139
chr2:17,082,892-19,555,672	Loss	2472781	p24.2 - p24.1	129
chr2:47,871,668-47,913,372	Loss	41705	p16.3	26
chr2:96,685,923-98,987,015	Gain	2301093	q11.2	122
chr2:98,987,015-99,310,234	High copy gain	323220	q11.2	21
chr2:99,310,234-115,209,148	Gain	15898915	q11.2 - q14.1	891
chr2:115,209,148-115,389,211	High copy gain	180064	q14.1	11
chr2:115,389,211-124,331,966	Gain	8942756	q14.1 - q14.3	473
chr2:124,331,966-125,952,676	High copy gain	1620711	q14.3	89
chr2:147,977,155-148,340,965	Homozygous copy loss	363811	q22.3	16
chr2:160,098,019-160,395,597	Loss	297579	q24.2	19
chr2:200,685,674-201,878,147	Loss	1192474	q33.1	102
chr2:211,746,930-232,604,377	Gain	20857448	q34 - q37.1	1322
chr2:232,604,377-232,810,269	High copy gain	205893	q37.1	13
chr2:232,810,269-242,118,949	Gain	9308681	q37.1 - q37.3	591
chr3:4,499,856-4,714,317	Loss	214462	p26.2	13
chr3:15,760,147-30,673,114	Gain	14912968	p24.3 - p24.1	847
chr3:32,894,032-36,997,480	Gain	4103449	p22.3 - p22.2	218
chr3:46,704,902-75,717,747	Loss	29012846	p21.31 - p12.3	1868
chr3:96,119,738-131,498,439	Loss	35378702	q11.2 - q21.3	2074
chr3:133,661,863-144,156,885	Loss	10495023	q22.1 - q23	698
chr3:154,366,004-199,501,827	Loss	45135824	q25.2 - q29	2836
chr4:30,928,350-48,818,171	Gain	17889822	p15.1 - p11	1029
chr4:48,818,171-49,324,512	Loss	506342	p11	13
chr4:52,379,976-54,001,926	Gain	1621951	q11 - q12	115
chr4:54,001,926-55,601,951	Loss	1600026	q12	141
chr4:57,756,781-58,477,891	Loss	721111	q12	36
chr4:59,282,223-84,667,611	Loss	25385389	q13.1 - q21.23	1379
chr4:84,667,611-86,334,752	Gain	1667142	q21.23	91
chr4:86,334,752-90,572,723	High copy gain	4237972	q21.23 - q22.1	291
chr4:90,572,723-92,216,636	Gain	1643914	q22.1	94
chr4:92,216,636-116,617,534	Loss	24400899	q22.1 - q26	1401
chr4:150,282,711-156,335,243	High copy gain	6052533	q31.23 - q32.1	408
chr4:174,686,909-176,738,183	Gain	2051275	q34.1 - q34.2	107
chr4:180,929,325-183,265,266	High copy gain	2335942	q34.3 - q35.1	115
chr4:189,587,206-191,040,830	Loss	1453625	q35.2	84
chr5:72,172,204-76,597,348	Loss	4425145	q13.2 - q14.1	254
chr5:85,672,364-86,090,775	High copy gain	418412	q14.3	22
chr5:130,374,979-142,235,475	Loss	11860497	q23.3 - q31.3	763
chr5:172,636,434-180,857,866	Homozygous copy loss	8221433	q35.2 - q35.3	452
chr6:0-44,324,035	Loss	44324036	p25.3 - p21.1	2863
chr6:44,324,035-44,330,142	Gain	6108	p21.1	17
chr6:44,330,142-46,756,760	Loss	2426619	p21.1 - p12.3	147
chr6:46,756,760-49,038,560	High copy gain	2281801	p12.3	127
chr6:49,038,560-55,583,943	Gain	6545384	p12.3 - p12.1	369

Table IV. *Continued*

Table IV. *Continued*

Chromosomal region	Copy number aberration	Length (bp)	Cytoband	No. of probes
chr6:55,583,943-57,048,799	High copy gain	1464857	p12.1	91
chr6:58,733,711-58,827,870	Loss	94160	p11.1	5
chr6:74,906,801-107,152,528	High copy gain	32245728	q13 - q21	1733
chr6:130,196,488-133,067,603	Gain	2871116	q22.33 - q23.2	153
chr6:135,489,105-135,956,121	Loss	467017	q23.3	44
chr6:137,243,750-137,499,193	Gain	255444	q23.3	15
chr7:0-1,121,607	High copy gain	1121608	p22.3	53
chr7:1,121,607-7,035,288	Gain	5913682	p22.3 - p22.1	446
chr7:7,035,288-16,220,801	High copy gain	9185514	p22.1 - p21.1	531
chr7:16,220,801-17,144,093	Gain	923293	p21.1	53
chr7:17,144,093-17,274,506	High copy gain	130414	p21.1	7
chr7:17,274,506-57,931,426	Gain	40656921	p21.1 - p11.1	2454
chr7:61,060,634-73,060,264	Gain	11999631	q11.1 - q11.23	641
chr7:75,463,022-91,853,628	Gain	16390607	q11.23 - q21.2	1061
chr7:92,385,908-98,849,814	Gain	6463907	q21.2 - q22.1	392
chr7:102,194,682-108,995,676	Gain	6800995	q22.1 - q31.1	404
chr7:108,995,676-109,629,306	High copy gain	633631	q31.1	38
chr7:110,609,962-111,191,239	High copy gain	581278	q31.1	34
chr7:138,278,951-140,733,077	Loss	2454127	q34	155
chr7:141,028,260-141,716,184	Loss	687925	q34	43
chr7:141,716,184-142,001,388	Homozygous copy loss	285205	q34	34
chr7:142,001,388-158,821,424	Loss	16820037	q34 - q36.3	1033
chr8:6,939,167-8,140,313	Loss	1201147	p23.1	42
chr8:51,018,695-51,876,043	Gain	857349	q11.22	50
chr8:52,319,845-56,579,297	Loss	4259453	q11.22 - q12.1	313
chr8:75,594,717-75,816,663	Loss	221947	q21.11	13
chr8:100,169,590-100,592,848	Loss	423259	q22.2	26
chr8:111,840,142-112,654,585	Gain	814444	q23.2 - q23.3	39
chr9:0-21,791,953	Loss	21791954	p24.3 - p21.3	1323
chr9:22,331,315-47,059,042	Loss	24727728	p21.3 - p11.1	1193
chr9:101,646,358-102,093,247	Loss	446890	q31.1	35
chr9:133,061,462-133,365,057	High copy gain	303596	q34.13	36
chr10:0-15,888,483	Loss	15888484	p15.3 - p13	952
chr10:16,915,490-36,318,413	Loss	19402924	p13 - p11.21	1177
chr10:36,593,683-37,866,631	Loss	1272949	p11.21	64
chr10:41,927,663-42,119,299	Gain	191637	q11.1 - q11.21	9
chr10:46,207,943-48,328,997	Gain	2121055	q11.22	81
chr10:49,279,264-51,016,781	Gain	1737518	q11.22 - q11.23	95
chr10:51,592,423-71,893,858	Gain	20301436	q11.23 - q22.1	1183
chr10:77,740,437-79,305,369	Gain	1564933	q22.3	91
chr10:89,615,986-89,851,240	Loss	235255	q23.31	25
chr10:89,851,240-104,145,580	Gain	14294341	q23.31 - q24.32	889
chr10:106,426,059-114,163,946	Gain	7737888	q25.1 - q25.2	445
chr10:114,163,946-124,316,045	Loss	10152100	q25.2 - q26.13	598
chr10:124,382,777-135,374,737	Loss	10991961	q26.13 - q26.3	652
chr11:0-3,759,910	Loss	3759911	p15.5 - p15.4	395
chr11:3,759,910-4,116,151	Homozygous copy loss	356242	p15.4	25
chr11:4,116,151-51,407,929	Loss	47291779	p15.4 - p11.11	2735
chr11:54,691,084-56,019,679	Loss	1328596	q11	79
chr11:56,348,485-111,109,293	Loss	54760809	q11 - q23.1	3569
chr11:111,109,293-111,379,863	Gain	270571	q23.1	15
chr11:111,379,863-134,452,384	Loss	23072522	q23.1 - q25	1626
chr12:10,914,787-11,201,643	Loss	286857	p13.2	17
chr12:11,201,643-11,831,298	High copy gain	629656	p13.2	39
chr12:33,409,429-35,400,000	Loss	1990572	p11.1 - q11	57
chr12:100,808,565-101,022,195	Gain	213631	q23.2	13
chr13:17,928,209-34,651,641	High copy gain	16723433	q11 - q13.2	1132
chr13:34,651,641-34,923,584	Gain	271944	q13.2 - q13.3	17

Table IV. *Continued*

Table IV. *Continued*

Chromosomal region	Copy number aberration	Length (bp)	Cytoband	No. of probes
chr13:34,923,584-49,660,630	High copy gain	14737047	q13.3 - q14.3	927
chr13:49,660,630-49,890,816	Gain	230187	q14.3	14
chr13:49,890,816-114,142,980	High copy gain	64252165	q14.3 - q34	3468
chr14:19,242,599-19,473,021	Loss	230423	q11.2	13
chr14:19,758,344-21,385,999	Loss	1627656	q11.2	127
chr14:21,385,999-21,678,310	Gain	292312	q11.2	34
chr14:21,678,310-22,073,646	Homozygous copy loss	395337	q11.2	43
chr14:22,073,646-54,510,912	Loss	32437267	q11.2 - q22.3	1849
chr14:61,276,314-88,287,948	High copy gain	27011635	q23.2 - q31.3	1613
chr14:88,287,948-90,535,004	Gain	2247057	q31.3 - q32.12	132
chr14:98,445,434-105,601,857	High copy gain	7156424	q32.2 - q32.33	526
chr14:105,700,924-106,368,585	High copy gain	667662	q32.33	40
chr15:20,145,866-30,712,202	Loss	10566337	q11.2 - q13.3	545
chr15:63,566,907-63,826,238	Loss	259332	q22.31	16
chr16:0-1,998,049	Gain	1998050	p13.3	122
chr16:2,074,844-23,832,350	Gain	21757507	p13.3 - p12.1	1434
chr16:23,832,350-24,085,795	Loss	253446	p12.1	15
chr16:24,085,795-29,582,504	Gain	5496710	p12.1 - p11.2	305
chr16:29,582,504-33,746,468	Loss	4163965	p11.2	227
chr16:33,746,468-35,006,622	Gain	1260155	p11.2 - p11.1	58
chr16:44,945,309-55,455,741	Gain	10510433	q11.2 - q13	647
chr16:56,876,211-76,791,921	Gain	19915711	q21 - q23.1	1270
chr16:77,529,554-88,827,254	Gain	11297701	q23.1 - q24.3	718
chr17:4,964,674-5,005,652	Loss	40979	p13.2	53
chr17:6,030,004-6,459,217	Loss	429214	p13.2	25
chr17:20,079,654-20,634,224	Loss	554571	p11.2	28
chr17:22,200,000-70,815,509	Loss	48615510	q11.1 - q25.1	3395
chr17:74,616,873-75,422,920	Loss	806048	q25.3	39
chr18:19,868,443-20,151,388	Loss	282946	q11.2	17
chr19:10,645,176-10,984,732	Loss	339557	p13.2	46
chr19:47,876,805-48,456,771	Loss	579967	q13.31	27
chr19:51,972,368-55,041,795	Loss	3069428	q13.32 - q13.33	206
chr19:55,041,795-59,364,356	Gain	4322562	q13.33 - q13.42	362
chr19:59,364,356-59,743,803	High copy gain	379448	q13.42	23
chr19:59,743,803-63,811,651	Gain	4067849	q13.42 - q13.43	242
chr20:7,042,589-8,048,700	High copy gain	1006112	p12.3	56
chr20:27,100,000-28,266,142	Gain	1166143	q11.1	10
chr20:29,297,076-39,079,714	Loss	9782639	q11.21 - q12	714
chr20:39,079,714-39,209,853	Homozygous copy loss	130140	q12	19
chr20:39,209,853-62,435,964	Loss	23226112	q12 - q13.33	1760
chr22:14,433,500-18,072,209	Gain	3638710	q11.1 - q11.21	238
chr22:18,529,725-28,719,750	Gain	10190026	q11.21 - q12.2	730
chr22:28,719,750-29,265,348	Loss	545599	q12.2	33
chr22:29,265,348-40,253,100	Gain	10987753	q12.2 - q13.2	846
chr22:44,546,688-44,803,212	High copy gain	256525	q13.31	16
chrX:0-59,500,000	Loss	59500001	p22.33 - q11.1	3431
chrX:61,697,828-95,798,355	Loss	34100528	q11.1 - q21.33	1923
chrX:95,798,355-96,306,484	Homozygous copy loss	508130	q21.33	33
chrX:96,306,484-101,646,251	Loss	5339768	q21.33 - q22.1	288
chrX:101,646,251-154,913,754	Homozygous copy loss	53267504	q22.1 - q28	3033

highest number of breakpoints were observed on chromosomes 1 and 4, whereas chromosomes 18 and 21 had the lowest; in fact, there were no unbalanced breakpoints on chromosome 21 and only two on chromosome 18. The long arm of chromosome 4 had a complex pattern of alternating copy number changes (Figure 4C), which is compatible with chromothripsis (47). Chromothripsis has been invoked to explain clusters of gross chromosomal rearrangements in a

wide variety of tumor types (48-52) but has not previously been described in a CPT-resistant cell line.

The detailed karyotype findings and the highly significant number of increased DNA break points generated in CPT-K5 cells not only indicates that the prolonged CPT inhibition of TOP1 at sublethal cellular doses is associated with the acquisition of major chromosomal and genomic reorganization both in terms of numerical and structural aberrations, but also that some chromosomes are unaffected. Absence of genomic or chromosomal aberrations suggests that these chromosomes or chromosomal regions might be lacking CPT-involved targets, and that these chromosomes or regions may contain genes of importance so only cells without aberrations affecting these genes may survive or that they have been repaired with great accuracy. This could be due to the essential functions of genes in those regions. The acquisition of major chromosomal reorganizations may at some point have resulted from DSBs, which in turn may have resulted from formation of TOP1-cc that were repaired erroneously, giving rise to copy number alterations, perhaps providing selective growth advantages.

Genomic copy number changes in CPT-K5 cells. To specifically address gene dosage changes that might be involved in generating highly stable CPT resistance, we closely examined different chromosomal locations harboring genes that are known to be involved in maintaining cellular and genomic homeostasis (53). Resistance of cancer cells to CPT is multifactorial, and five major mechanisms may account for cellular CPT resistance (6, 53-55): i) reduced TOP1 activity, either by reduced specific activity or a reduced cellular amount *e.g.* due to reduced gene dosage; ii) *TOP1* mutations that render the enzyme drug-resistant; iii) reduced intracellular active drug content by decreased drug influx or increased drug efflux; iv) resistance to apoptosis; and v) efficient repair of TOP1-cc by the cell.

A first line of defense for a cell against CPT-induced damage is down-regulation of its TOP1 activity, thereby reducing TOP1-cc (55, 56). Our subtractive oligo-based aCGH analysis revealed that the gene dosage of the *TOP1* locus was diminished by a factor of approximately 1.7, which was confirmed by FISH (Figure 5). The loss of *TOP1* gene copy numbers correlated with a reduced level of cellular TOP1 protein in CPT-K5 cells (Figure 2). Other studies have shown that a copy number change of the *TOP1* gene correlates with the cellular amount of enzyme and seems to be a common mechanism contributing to CPT resistance (56). By CGH analysis of the CPT-resistant cell lines HT-29/CPT, A549/CPT and st-4/CPT, a reduced DNA copy number of TOP1 was shown together with a reduced relative expression of TOP1 (44). In our subtractive oligo-based aCGH analysis, we further screened for copy number changes of other type I topoisomerases (*TOP1MT, TOP3A* and *TOP3B*) and type II topoisomerases (*TOP2A, TOP2B* and *TOPOVIA* (also known as *S. cerevisiae*, homolog of, *SPO11*). We observed that *TOP2A* and *SPO11* exhibited large losses, and loci of TOP3B and TOP2B were gained, while *TOP3A* and *TOP1MT* displayed no copy number change between the CPT-K5 and RPMI-8402 cells (Table IV).

Another line of defense for a cell to resist the effects of CPT is through the acquisition of single nucleotide mutations of *TOP1* thereby preventing the action of CPT on TOP1-cc [reviewed in (57)] (Table III). We previously showed that CPT-K5 harbors mutated *TOP1* containing the Asp533Gly mutation (34). These types of mutations, however, cannot be revealed by oligo-based aCGH analysis.

Reduced intracellular CPT concentration is a third important way to reduce the formation of devastating TOP1-cc. One of the major mechanisms responsible for multidrug resistance in cancer chemotherapy is overexpression of some members of the ATP-binding cassette (ABC) transporter superfamily, including ABCB1, ABCC1 and ABCG2, resulting in decreased intracellular levels of drugs [reviewed in (58)]. In mammalian cells, expression of ABC transporters such as Pgp (ABCB1) and ABCG2 confers resistance to CPT and its derivatives (59-61). Gene amplification is a major contributor to increased

→

Figure 5. *Fluorescence in situ hybridization (FISH) validation of copy number changes at specific genomic regions important for the camptothecin resistance in CPT-K5 cells. Left hand-side panel: Genomic profiles of chromosome 20 (upper panel), chromosome 4 (middle panel) and chromosome 14 (lower panel) together with their respective ideograms beneath. Magnified genomic profile views of corresponding altered chromosomal regions are given below chromosome 20, chromosome 4, and chromosome 14 indicating deleted region at 20q12 containing topoisomerase 1 (TOP1) gene, highly amplified region at 4q22.1 containing ATP-binding cassette sub-family G member 2 (ABCG2) gene and amplified region at 14q31.3q32.11 containing the tyrosyl-DNA phosphodiesterase 1 (TDP1) gene, respectively. Blue and red bars around the ideograms indicate regions of gains and losses, respectively. Regions with high gains and losses are indicated by double bars in their respective color. A yellow bar in the copy number profile of chromosome 14 indicates the region of gain in the CR1-CR2/MMRU cell lines (see Table III). Right hand-side panel: FISH analyses confirm the genomic array comparative genomic hybridization (aCGH) findings in the RPMI-8402 and CPT-K5 cell lines on interphase nuclei with hybridization signals using the following probe sets as indicated by red and green marks on the respective ideograms in the left hand-side panel: i) Bacterial artificial chromosome (BAC)-based probe containing the TOP1 gene (red) and centromere 20 probe (green); ii) BAC-based probe RP11-368G2 (green) containing the ABCG2 gene together with centromere 4 probe (red) – to the right metaphase spreads represented by partial karyograms of chromosomes 4 and 12; and iii) BAC-based probe RP11-213O13 (red) containing the TDP1 gene together with subtelomeric 14-qter probe (green) - to the right metaphase spreads represented by partial karyograms of derivative chromosomes 11 (der(11)t(11;14)) and 15 (der(15)t(14;15)) for RPMI-8402 and partial karyograms of derivative chromosomes 5 (der(5)t(5;14)(q35;q32)) and 14 for CPT-K5.*

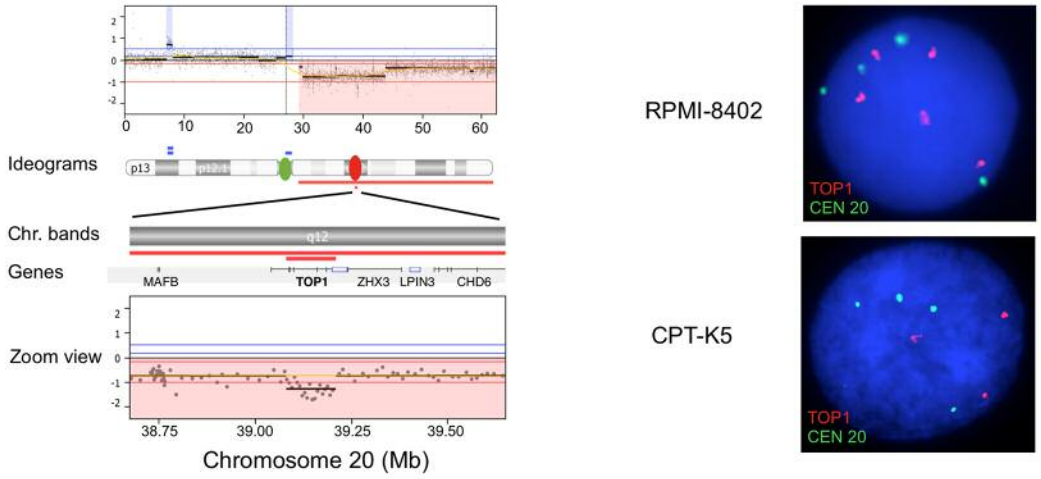
Ideograms
Chr. bands
Genes
MAFB
TOP1
ZHX3
LPIN3
CHD6
Zoom view
Chromosome 20 (Mb)
RPMI-8402
TOP1
CEN 20
CPT-K5
TOP1
CEN 20

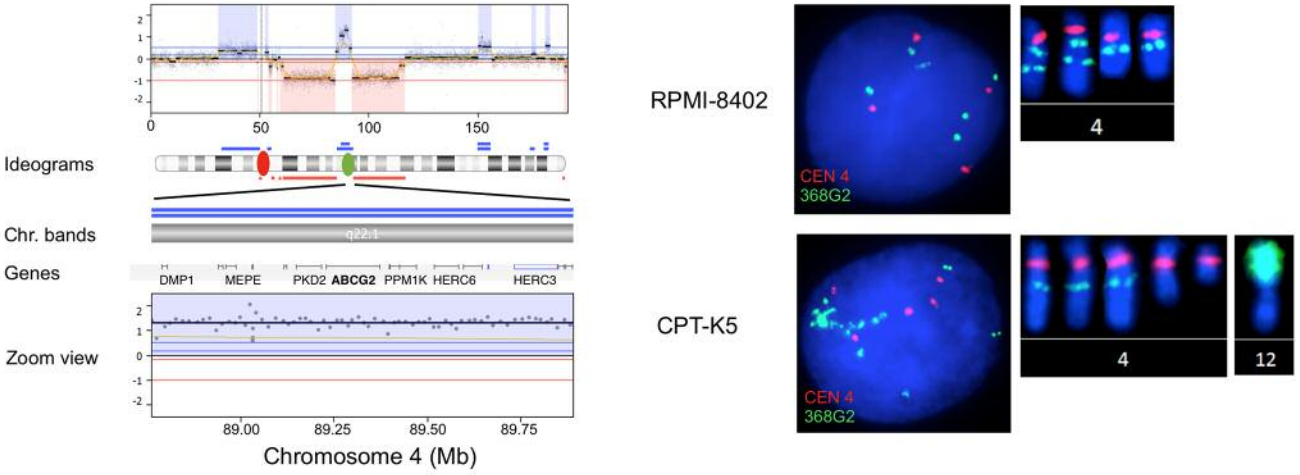
Ideograms
Chr. bands
Genes
DMP1
MEPE
PKD2
ABCG2
PPM1K
HERC6
HERC3
Zoom view
Chromosome 4 (Mb)
RPMI-8402
CEN 4
368G2
4
CPT-K5
CEN 4
368G2
4
12

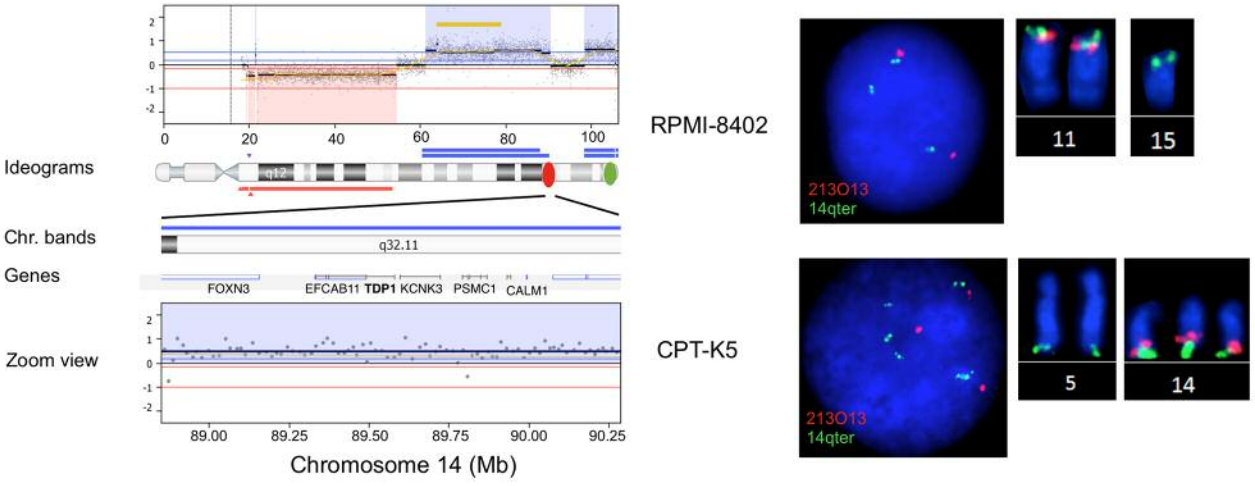
Ideograms
Chr. bands
q32.11
Genes
FOXN3
EFCAB11
TDP1
KCNK3
PSMC1
CALM1
Zoom view
Chromosome 14 (Mb)
RPMI-8402
213O13
14qter
11
15
CPT-K5
213O13
14qter
5
14

Table V. *Copy number findings of key genes involved in DNA repair pathways and cell-cycle arrest in CPT-K5 cells relative to RPMI-8402 cells.*

HGNC-approved gene symbol	Function	Cytoband	Pos. (hg18)	Copy number
Proteasome-dependent TOP1 degradation pathway/phosphodiesterase pathway for TOP1-cc repair of single-ended DSB				
PARP1	DSB recognition, *XRCC1* and *TDP1* recruitment	1q42.12	224,615,015-224,662,424	Loss
TDP1	Hydrolyze the tyrosyl-DNA link in Top1-DNA complex	14q32.11	89,491,999-89,580,861	High gain
XRCC1	DNA binding	19q13.31	48,739,304-48,771,570	nc
PTEN	Phosphatase, negative regulator of PI3K/AKT pathway	10q23.31	89,613,175-89,718,512	Loss
PNKP	End processing	19q13.33	55,056,273-55,062,630	Gain
APEX1 or *APE1*	Apurinic/apyrimidinic endodeoxyribonuclease 1	14q11.2	19,993,130-19,995,766	Loss
POLB	DNA polymerase beta	8p11.21	42,315,187-42,348,470	nc
PRKDC		8q11.21	48,848,222-49,035,296	nc
Proteasome-independent pathway/endonuclease pathway for TOP1-cc repair of single-ended DSB				
ERCC1	Interacts with ERCC4 to form endonuclease	19q13.32	50,608,532-50,618,642	nc
ERCC4 or *XPF*	3'-Flap endonuclease subunit	16p13.12	13,921,515-13,953,706	Gain
RPA1	Replication protein A1 subunit	17p13.3	1,680,023-1,749,598	nc
RPA2	Replication protein A2 subunit	1p35.3	28,090,636-28,223,823	nc
RPA3	Replication protein A3 subunit	7p21.3	7,643,100-7,724,763	High gain
POLD1	Polymerase delta catalytic subunit A	19q13.33	55,579,405-55,613,083	Gain
POLD2	Polymerase delta catalytic subunit B	7p13	44,120,811-44,129,672	Gain
POLD3	Polymerase delta catalytic subunit D	11q13.4	73,981,277-74,031,413	Loss
POLD4	Polymerase delta catalytic subunit A	11q13.1	66,875,595-66,877,593	Loss
FEN1	Flap structure-specific endonuclease 1	11q12.2	61,316,726-61,321,286	Loss
LIG1	DNA ligase 1	19q13.32	53,130,515-53,365,372	Loss
SLX4	Structure-specific endonuclease subunit	16p13.3	3,571,185-3,601,608	Gain
HR & NHEJ				
ATM	Binds to MRN complex, phosphorylates *CHK2*	11q22.3	107,598,769-107,745,036	Loss
H2AFX	Activated by ATM, recruit further DNA repair components	11q23.3	118,469,795-118,471,387	Loss
MRE11	Endonuclease, 3'-5' exonuclease, MRN complex	11q21	93,790,115-93,866,688	Loss
NBN or *NBS1*	Adaptor, check point roles, MRN complex	8q21.3	91,014,740-91,060,075	nc
PARP1	DSB recognition, MRN complex recruitment	1q42.12	224,615,015-224,662,424	Loss
RAD50	ATPase/Scaffold, MRN complex	5q31.1	131,920,529-132,007,494	Loss
HR				
BARD1	BRCA1-associated ring domain	2q35	215,301,520-215,382,673	Gain
BLM or *RECQL3*	Bloom syndrome, helicase	15q26.1	89,061,583-89,159,690	Gain
BRCA1	Mediator/adaptor, ubiquitin ligase	17q21.31	38,449,840-38,530,994	Loss
BRCA2	Recombination mediator, binds to RAD51	13q13.1	31,787,617-31,871,809	High gain
RBBP8 or *CtIP*	Endonuclease; binds to BRCA1	18q11.2	18,767,293-18,860,447	nc
DNA2	DNA replication helicase 2	10q21.3	69,843,827-69,901,885	Gain
EXO1	5'-3' Exonuclease	1q43	240,078,158-240,119,671	Loss
LIG1	ATP-dependent DNA ligase	19q13.32	53,310,515-53,365,372	Loss
PALB2	Partner and localizer of BRCA2	16p12.1	23,521,984-23,560,179	Gain
POLD	See above for *POLD1-4*	-	-	-
POLE	Catalytic subunit DNA polymerase epsilon	12q24.33	131,710,421-131,774,018	nc
RAD51	Recombinase, homology pairing	15q15.1	38,774,651-38,811,648	nc
RAD52	Mediator of repair	12p13.33	904,877-912,503	nc
ATRX or *RAD54*	Recombinase, D-loop formation	Xq21.1	76,647,012-76,928,375	Loss
RPA	See above for *RPA1-3*	-	-	-
Classic NHEJ				
APTX	End processing	9p13.3	32,962,608-32,991,626	Loss
APLF	End processing	2p14	68,548,246-68,660,798	nc
LIG4	DNA ligase 4, complexes with *XRCC4*	13q33.3	107,657,793-107,665,883	High gain
NHEJ1 or *XLF*	Scaffold protein	2q35	219,648,290-219,733,831	Gain
PNKP	End processing	19q13.33	55,056,273-55,062,630	Gain
PRKDC or *DNA-PKcs*	DSB-responsive PIKK family protein kinase	8q11.21	48,848,222-49,035,296	nc
POLL or *DNA-Pol μ*	End processing, gap filling	10q24.32	103,328,629-103,337,963	Gain
POLM or *DNA-Pol μ*	End processing, gap filling	7p13	44,078,372-44,088,607	Gain
XRCC4	Scaffold protein	5q14.2	82,409,073-82,685,335	nc
XRCC5 or *Ku80*	dsDNA end binding, resection inhibition	2q35	216,682,377-216,779,248	Gain
XRCC6 or Ku70	dsDNA end binding, resection inhibition	22q13.2	40,347,241-40,389,998	nc

Table V. *Continued*

Table V. *Continued*

HGNC-approved gene symbol	Function	Cytoband	Pos. (hg18)	Copy number
Alternative NHEJ				
RBBP8 or *CtIP*	Nuclease; binds to BRCA1	18q11.2	18,767,293-18,860,447	nc
POLB	Gap filling	8p11.21	42,315,187-42,348,470	nc
XRCC1	DNA binding	19q13.31	48,739,304-48,771,570	nc
LIG3	DNA ligase 3, complexes with *XRCC1*	17q12	30,331,651-30,356,201	Loss
WRN	DSB repair mediator, Helicase 3'-5 exonuclease	8p12	31,010,320-51,150,819	nc
Mismatch repair				
MLH1	Forms a heterodimer with PSM2	3p22.2	37,009,983-37,067,341	nc
MLH3	Forms heterodimer with MLH1	14q24.3	74,550,220-74,587,988	High gain
MSH2	Forms heterodimer with MSH6	2p16.3	47,483,767-47,563,864	nc
MSH3	Forms heterodimer with MSH3	5q14.1	79,986,050-80,208,390	nc
MSH6	Forms heterodimer with MSH2	2p16.3	47,863,725-47,887,596	Loss
PMS1	Forms heterodimer with MLH1	2q32.2	190,357,056-190,450,600	nc
PMS2	Forms heterodimer with MLH1	7p22.1	5,979,396-6,015,263	Gain
Cell-cycle arrest				
CHK1	Phosphorylated by ATR, G_2/M cell-cycle arrest	11q24.2	125,001,854-125,030,850	Loss
CHK2	Phosphorylated by ATM, G_1 cell-cycle arrest	22q12.1	27,413,731-27,460,715	Gain
TP53	G_1 and G_2 Cell cycle arrest	17p13.1	7,512,445-7,531,588	nc

DSB: Double=strand break HR: homologous recombination; NHEJ: non-homologous end-joining; nc: no change.

expression of ABCB1 and ABCG2 in colorectal and breast cancer cells making them resistant towards the CPT-analog SN-38 and mitoxantrone (62, 63). Remarkably, we found that in the CPT-K5 cell line, the genes *ABCB1* and *ABCC1* are located in regions of copy number gain at 7q21.12 and 16p13.11, respectively, while *ABCG2* is in the region of highest copy gain at 4q22.1 (Figure 5, Table IV). The CPT-resistant cell lines HT-29/CPT and A549/CPT had amplified ABC transporter family genes (44). These observations indicate that copy numbers gains of ABC transporters are of importance in decreased intracellular CPT accumulation in CPT-K5 cells. It has been shown that CPT-K5 is multidrug resistant *e.g.* it is also resistant to topoisomerase II inhibitors (64). This observation is in line with the findings that there are many drugs that are substrates for the ABCG2 transporter, including topoisomerase II inhibitors (*e.g.* mitoxantrone, etoposide, daunorubicin, and doxorubicin), CPT analogs (*e.g.* topotecan, and irinotecan), tyrosine kinase inhibitors, antimetabolites, and many other drug types [reviewed in (58)]. Interestingly, a glioblastoma cell line, SF295, which became mitoxantrone-resistant by exposure to step-wise increasing concentrations of the drug had a resulting *ABCG2* amplification by forming double minutes, which were later reintegrated into the genome at multiple chromosomal regions during subsequent selection steps (43). In the CPT-K5 cell line, we found that the *ABCG2* gene in addition to its location at 4q22.1 is highly amplified at a single chromosomal site on der(12)t(4;12) (Figure 5), suggesting a similar mechanism of amplification to that observed in the SF295 cell line. Taken together, these findings support the idea that *ABCG2* is one of the most important transporter genes in relation to CPT and its derivatives, which is in agreement with previous suggestions (65-67).

Alteration of apoptotic pathways is a fourth line of defense in influencing resistance to CPT. The biochemical pathways of apoptosis include pro-apoptotic and anti-apoptotic proteins, which affect the cellular response to CPT as reviewed elsewhere (7, 68). A delicate balance between pro- and anti-apoptotic pathways has been proposed to provide alternative means of providing cancer cells with a selective advantage promoting chemoresistance (69). Apoptosis involves a complex network of many proteins of which the proteins encoded by tumour protein p53 (*TP53*), inhibitor of apoptosis, X-linked (*XIAP*) and baculoviral IAP repeat-containing protein 5 (*BIRC5*) play important roles in regulating apoptosis (70). TP53 plays an important role in sensitivity to CPT and apoptosis induced by CPT. When leukemia cells are deficient in p53 function, the cells are hypersensitive to CPT, whereas cells with normal functioning p53 are resistant to CPT (71, 72). In our study, we found that the copy number of *TP53* was unchanged (Tables IV and V), which is in agreement with previous findings that normal TP53 is important for resistance to CPT and its derivatives. The anti-apoptotic genes *XIAP* and *BIRC5* possess a wide range of biological activities that promote cancer cell survival and proliferation to overcome endogenous and exogenous insults [reviewed in (68)]. We found CPT-K5 cells had loss of the *XIAP* gene and that *BIRC5* had no copy number change (Table IV).

A fifth line of defense against CPT is efficient repair of CPT-induced DNA damage by the cell (53). Although the

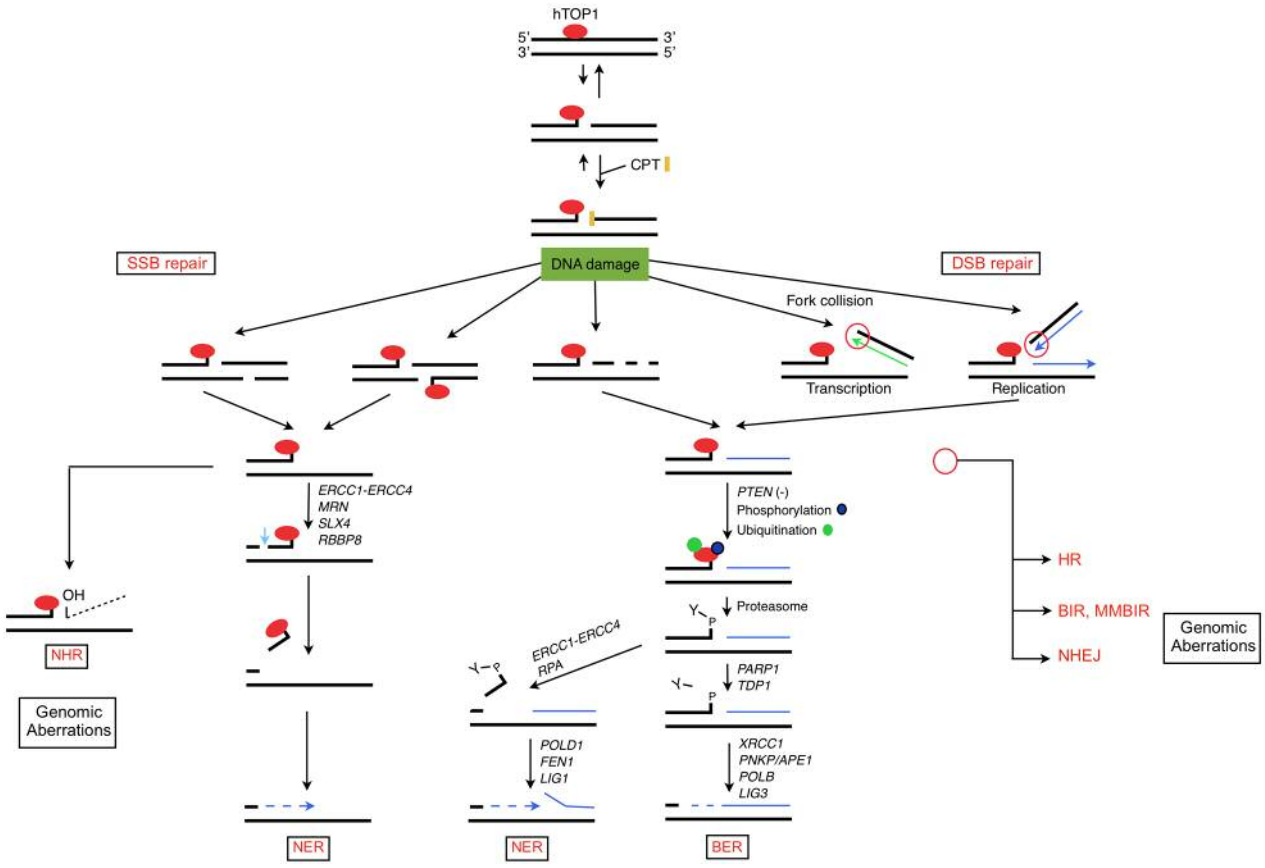

Figure 6. *Schematic overview of mechanisms implicated in repair of camptothecin (CPT)-induced DNA damage. BER: Base excision repair; BIR: breakage-induced replication; CPT: camptothecin or its derivatives; DSB: double-strand break; HR: homologous recombination; MMBIR: micro-homology-mediated BIR; MRN: meiotic recombination 11 (MRE11)/DNA repair protein RAD50(RAD50)/nibrin (NBS1) complex; NER: nucleotide excision repair; NHEJ: non-homologous end-joining; NHR: non-homologous recombination; PTEN(−) indicates phosphatase and tensin homolog deficiency; SSB: single-strand DNA break. Open red circle indicates fork collision and repair mechanisms; Y-P: 3'-phosphotyrosyl.*

mechanisms implicated in repair of TOP1-cc have been widely studied they still remain largely elusive (73-78). The repair of this rather unique form of DNA damage involves different pathways (Figure 6) that cooperate to remove the TOP1-cc and restore intact DNA, thus allowing the resumption of physiological cellular functions including replication and transcription. An important step in the repair of TOP1-cc is degradation of DNA-bound TOP1 (76). Furthermore, it has been shown that cells that rapidly degrade TOP1 are resistant to CPT, while cells that fail to degrade TOP1 are sensitive to CPT (75, 79). TOP1 covalently stalled on DNA is degraded *via* a ubiquitin-26S proteasome pathway into a small peptide with a tyrosyl residue attached to the 3'-end of the nicked DNA (75, 76). A recent finding suggests that phoaphatase and tensin homolog (PTEN) availability may determine the fate of cells harboring CPT-induced DNA damage by regulating activity of DNA-dependent protein kinase (PRKDC) kinase, which phosphorylates TOP1 on serine 10 (79). It was found that *PTEN* deletion ensures higher TOP1 serine 10 phosphorylation leading to rapid TOP1 degradation and CPT resistance. PRKDC-dependent phosphorylation of TOP1 in complex with DNA seems to be a prerequisite for ubiquitinylation, which in turn is required for proteasomal degradation (79).

Another important aspect of the repair of CPT-induced DNA damage is the fate of stalled or collapsed replication or transcription fork complexes which are generated by CPT (80). Colliding replication forks on the leading strand for DNA synthesis or transcription on the template strand convert CPT-stabilized TOP1-cc into devastating DSBs if unrepaired. Break-induced replication (BIR) is a homologous recombination pathway which was recently identified as serving for repair of collapsed or broken replication forks [reviewed in (81, 82)]. Another more recent BIR-related pathway called micro-homology-mediated BIR has been proposed to explain copy number alterations, complex chromosomal rearrangements and microsatellite expansion

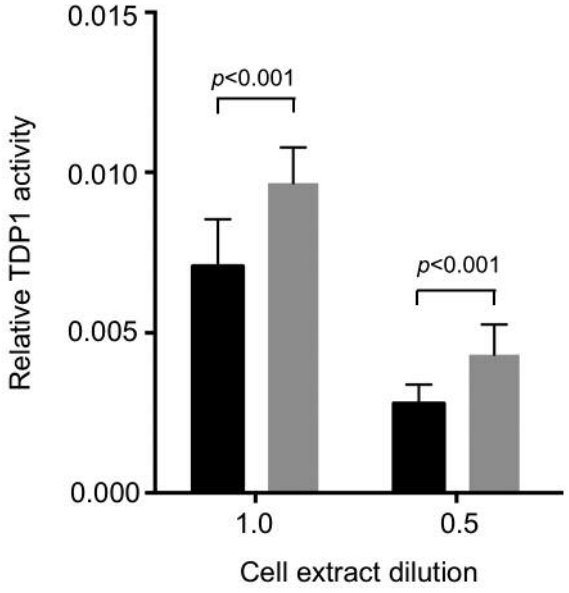

Figure 7. *Bar chart showing the mean of the results obtained when measuring relative tyrosyl-DNA phosphodiesterase 1 (TDP1) activity in whole-cell extracts from 1.0×10^6 and 0.5×10^6 RPMI-8402 (black bars) and CPT-K5 (grey bars) cells, as indicated in the figure, in three independent repetitions. Relative TDP1 activity in CPT-K5 cells was increased by a factor of 1.42 ($p<0.001$; unpaired t-test). The error bars indicate standard deviation.*

associated with cancer and various other diseases in humans (81-83). It is beyond the scope of this study to describe these processes in more detail, as excellent reviews exist (81, 82).

A summary of the genes involved in the repair processes described above is given in Table V, which also provides information about copy number changes affecting these genes in the CPT-K5 cell line. Interestingly, important genes involved in the repair of TOP1-induced DNA damage had copy number changes. Firstly, the *PTEN* gene, an upstream effector of the proteasomal pathway, had a copy number loss. Secondly, a 50% increase in copy number of the *TDP1* gene, which was confirmed by FISH analysis (Figure 5), and a 1.42-fold higher relative activity of TDP1 (Figure 7) were identified. Both of these observations are in agreement with the recent findings by Ando *et al*. (79) suggesting that *PTEN* deletion ensures higher TOP1 serine 10 phosphorylation by PRKDC, favoring rapid TOP1 degradation and CPT resistance. It might be interesting in future studies to determine PTEN expression or the level of phosphorylated serine 10 in TOP1 in the CPT-K5 cell line and investigate whether TOP1 is more degraded in response to CPT in CPT-K5 cells. A previous BAC-based aCGH analysis on the irinotecan-resistant cell lines CR1 and CR2, derived from parental melanoma MMRU cell lines, showed a gain of the region 14q23.2 to q31.1 (21). The amplified region in that study is within the region gained at 14q23.2-q32.12 observed in CPT-K5 cells (Table IV; Figure 5) but amplification in the CR1 and CR2 cells did not include the *TDP1* gene. A major difference between the CPT-K5 and the CR1/CR2 cell lines is that the latter needs CPT to be present for the cells to conserve their CPT resistance as opposed to CPT-K5 cells, which are stably CPT-resistant in the absence of CPT. This difference may influence the cellular dynamics of *e.g*. DNA repair.

The DNA mismatch repair (MMR) system also plays an important role in maintaining genomic stability (84). The main genes involved in MMR include, *E. coli* homolog of *MutL* (*MLH1*), *MLH2*, *E. coli* homolog of *MutS* (*MSH2*), *MSH3*, *MSH6*, postmeiotic segregation increased, *S. cerevisiae* 1 (*PMS1*), and *PMS2*. Defects in any of these genes result in microsatellite instability (85) and repeat expansions (86). It was shown in one study that *MSH2* deficiency results in a higher sensitivity to CPT, while loss of *MLH1* results in CPT resistance (87). In the CPT-K5 cell line, we observed a gain of *MLH3* and *PMS2*, and a 3'-partial loss of *MSH6*, while there were no copy number changes in the other MMR genes (Table V). Although only few studies exist on MMR and CPT sensitivity, gain of *MLH3* located at 14q24.3 might be a recurrent rearrangement in CPT-resistant cells as it was also observed in CPT-resistant MMRU cells (21).

A slower growth rate has been reported in several CPT-resistant cell lines (55, 11, 22), although this does not seem to be a major mechanism of resistance to TOP1 inhibitors (55). It may, however, be a reminiscence of altered properties as a result of obtaining CPT resistance because cell-cycle checkpoint arrest is important to allow time for repair and to prevent progression of replication. CPT-induced DNA damage activates *S. pombe* homolog of checkpoint 1 (CHK1) and CHK2 checkpoint kinases (88). The two independent CPT-resistant colorectal cancer cell lines derived from HT-29 and HCT-116 had an approximately 30% increased doubling time (22). Increased basal levels of H2A histone family, member X (γ-H2AX) and activated CHK2 accompanied these findings, without notable changes in the level of CHK1. Consistent with these findings, the CPT-K5 cell line has an increased generation doubling time (approximately 100% increase) (11) and amplification of the *CHK2* gene together with a relative loss of *CHK1* (Table V).

STR profiling of RPMI-8402 and CPT-K5. Because of the major cytogenetic and genomic differences between RPMI-8402 and CPT-K5 cells, we wanted to examine whether STRs differ between the two cell lines. STRs are microsatellites with repetitive sequences characterized by a variable number of repeated short sequence elements of 2-6 bp in length as a unit (*e.g*. di-, tri-, and tetra-sequences). They are highly polymorphic between individuals and are especially used in forensic studies for human identification, and more recently for authentication of human cell lines (89, 90).

Table VI. *Short tandem repeat (STR) profiling of RPMI-8402 and CPT-K5 cells using the AmpFISTR® Identifiler PCR amplification kit.*

STR locus	Chromosomal location	STR alleles[a]		Match	Repeat unit[b]
		RPMI-8402	CPT-K5		
TPOX*	2p25.3	8	8	M	$(AATG)_{6-14}$
D2S1338	2q35	19	23	m	$(TGCC)_6(TTCC)_{11}$
		23	24		
			26		
			(27)		
D3S1358	3p21.31	14	14	m	TCTA $(TCTG)_{2-3}(TCTA)_{10-15}$
		16	15		
			16		
FGA	4q28	23	21		$(TTTC)_3TTTTTTCT(CTTT)_7CTCC(TTCC)_2$
			22		
			24		
D5S818*	5q23.2	12	11	m	$(AGAT)_{7-15}$
		13	12		
			13		
CSF1PO	5q33.1	11	9	m	$(AGAT)_{5-16}$
		12	(10)		
			11		
			12		
D7S820*	7q21.11	8	9	None	$(GATA)_{6-14}$
		13	12		
			14		
D8S1179	8q24.13	11	13	None	$(TCTA)_{7-12}$
			14		
TH01	11p15.5	9	6	None	$(AATG)_{3-12}$
		9.3	7		
vWA	12p13.31	14	(17)	m	TCTA TCTG TCTA $(TCTG)_4$ $(TCTA)_3$
		20	18		
			20		
			22		
D13S317	13q31.1	12	10	m	$(TATC)_{7-15}$
			12		
D16S539	16q24.1	10	10	m	$(GATA)_{5-15}$
		11	14		
D18S51	18q21.33	16	14	None	$(AGAA)_{8-27}$
		20	17		
			18		
D19S433	19q12	12	14	m	$(AAGG)(AAAG)(AAGG)(TAGG)(AAGG)_{7-12}$
		(13)	15		
		14			
D21S11	21q21.1	30	28	m	$(TCTA)_4(TCTG)_6(TCTA)_3TA(TCTA)_3TCA$ $(TCTA)_2TCCATA(TCTA)_6$
			30		
			33.2		
			34.2		

M: Complete match, m:partial match, None: no match of genotypes. *Denotes STR loci analyzed by topoisomerase 1 (TOP1) DNA cleavage assay; [a]Numbers in brackets indicate a minor peak; [b]Subscripts indicate number of repeat units. A more detailed allele listing of these STR loci is available at www.cstl.nist.gov/biotech/strbase/fr_fact.htm.

The AmpFISTR® Identifiler PCR Amplification tests STR alleles (tetra-nucleotide repeats) at 15 loci that are located on distinct chromosomes, behave according to known principles of population genetics and contain low mutation rates [reviewed in (91)]. The results from the STR profiling analysis of RPMI-8402 and CPT-K5 cells are summarized in Table VI. A comparison of the STR results of the two cell lines shows that it is only the *TPOX* locus which has a complete match, with the homozygous STR allele bearing the eight repeat units present in both cell lines. For the remaining 14 STR loci, there was either a partial match (D2S1338, D3S1358, D5S818, CSF1PO, vWA, D13S317, D16S539, D19S433, D21S11) or

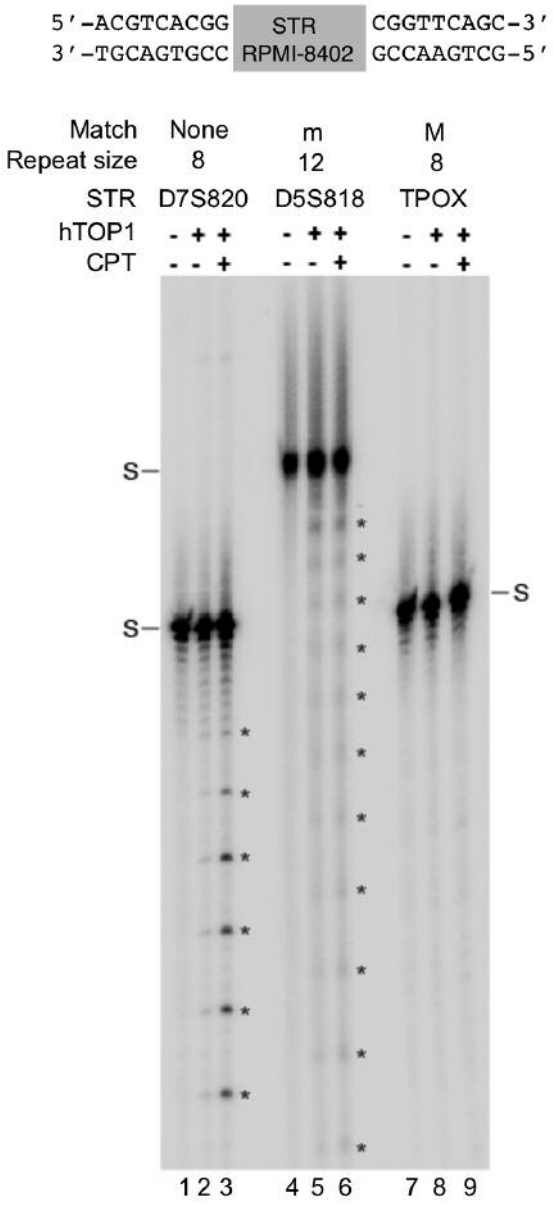

Figure 8. *Topoisomerase 1 (TOP1) DNA cleavage assay using short tandem repeat (STR) sequences as DNA substrate. The top panel shows the construction of the double-stranded oligonucleotide substrates. The grey box indicate the double-stranded STR alleles representing no match (None) D7S820, a partial match (m) D5S818, and a complete match (M) for thyroxin peroxidase (TPOX) as observed in the STR profiling of DNA from RPMI-8402 and CPT-K5 cell lines. These oligonucleotides were constructed so that the sequence of each of the three selected RPMI-8402 STR alleles were flanked by a common sequence identical in the three different substrates. Each construct was 5'-radiolabeled and subjected to human topoisomerase 1 (hTOP1) DNA cleavage with purified recombinant hTOP1 in the absence and presence of CPT before the products were separated by 12% polyacrylamide gel electrophoresis. Lanes 1, 4 and 7: incubation without enzyme and CPT; lanes 2, 5 and 8: incubation with hTOP1 in the absence of CPT; lanes 3, 6 and 9: incubation with hTOP1 and 10 μM CPT. Uncleaved substrates are marked (S) and *denotes hTOP1 DNA cleavage sites.*

no match (FGA, D7S820, D8S1179, TH01, D18S51) of the STR alleles between the two cell lines. The aberrant STR loci did not correlate with the observed differences in translocations or breakpoints as identified by karyotyping or genomic profiling. The total number of STR alleles increased from 26 in the RPMI-8402 cells to 42 in the CPT-K5 cell line ($p<0.01$), which is in line with the observed number of changes by karyotyping and by breakpoints identified by oligo-based aCGH analysis. These findings are in agreement with the fact that CPT induces genomic instability.

STRs can be cleaved in vitro by TOP1 and DNA cleavage can be stimulated by CPT. The most obvious conclusion from the STR data is that either the two cell lines are not related or alternatively that differences may be the result of CPT-induced DNA damage and repair.

To test whether STR alleles are targets for CPT-induced DNA damage, we performed a number of classical *in vitro* TOP1 DNA cleavage experiments in the presence and absence of the drug (Figure 8). We found that the substrate containing the sequence of the D7S820 locus was a stronger TOP1 DNA cleavage site than the substrate containing the sequence for the D5S818 locus in the absence of CPT. Addition of CPT to the TOP1 cleavage reaction resulted in very strong stimulation of DNA cleavage of the D7S820 STR substrate, whereas only very weak stimulation for the D5S818 STR substrate was observed. In contrast, the TPOX STR substrate was not cleaved by TOP1 and neither was cleavage stimulated by CPT.

Correlating these findings with the observed STR allelic differences between the two cell lines, it should be noted that the TPOX STR was the only allele that showed a complete match in the STR profiling and that we found only one allele in both cell lines. This finding indicates that because the TPOX STR does not contain a TOP1 cleavage site it is stable in the presence of CPT. Furthermore, the D7S820 locus, which did not exhibit any match in the STR profiling, contained the strongest TOP1 DNA cleavage site. This site was also the site with the strongest cleavage stimulation by CPT of the three loci sequences tested. Taken together, our findings indicate that the genomic stability of the tested STR alleles depends upon their ability to be cleaved by TOP1 and how strongly CPT can enhance this cleavage. This interpretation is in agreement with the studies on transcription-induced trinucleotide STR instability (92-94). Another way STR can become unstable or mutate is by replication strand slippage or misalignment (95). Replication fork collapse or arrest is one source of DNA strand slippage and as CPT greatly enhances the frequency of replication fork arrests, it is not unlikely that it will affect the STRs as exemplified by the tetra-nucleotides we examined. Normally the rate of slippage is highest in dinucleotide STRs and lowest in tetra-nucleotides but how CPT affects the rate of slippage remains unknown (96).

In conclusion, it is highly likely that cells subjected to continuous sublethal concentrations of CPT acquire increased STR instability, but further studies focusing on CPT and STR are warranted.

Conclusion

A major clinical problem is that initially responding patients with cancer treated with CPT or its derivatives gradually acquire resistance. We used the stably and highly CPT-resistant cell line CPT-K5 to obtain global genomic insight into acquired CPT resistance by characterizing the cell line, and its parental, using 24-color karyotyping and subtractive oligo-based aCGH analysis.

Although many human cell lines resistant to CPT or its derivatives have been developed, only very few of these have been examined at the chromosomal or genomic level. This is intriguing because CPT is a specific inhibitor of TOP1, which has a major role in DNA metabolism, such as in transcription, replication, recombination and repair.

By 24-color karyotyping, we showed that CPT-K5 is hypo-tetraploid with a modal chromosomal number reduced to 80, and had loss or gain of 18 structural aberrant chromosomes compared with its parental RPMI-8402. Subtractive oligo-based aCGH analysis identified 165 copy number alterations and 236 unbalanced DNA breakpoints unevenly distributed across the chromosomal complement in CPT-K5 cells. Furthermore, we found that STRs highly differ between CPT-K5 and its parental cell line, and we show for the first time that STRs are TOP1 targets that can be differentially stimulated by CPT. These findings are in agreement with repair pathways that efficiently repaired CPT-induced DNA damage at the expense of conserved genome integrity providing substantial chromosomal and genomic alterations that may have been beneficial for survival and cellular proliferation. However, further studies are needed to establish whether STR alterations actually contribute to cellular tolerance to CPT.

We suggest that acquired resistance to CPT in the CPT-K5 cell line is a multifactorial process. Four major mechanisms seem to be involved in addition to its acquired previously described *TOP1* mutation. These are: i) reduced gene dosage of *TOP1* resulting in decreased cellular amount and activity of the enzyme; ii) high amplification of *ABCG2*, which may contribute to reduced intracellular concentration of active drug by decreased drug influx/increased drug efflux; iii) no copy number changes in *TP53* and *BIRC5* genes, which may contribute to resistance to apoptosis; and iv) high amplification of *TDP1* accompanied by increased TDP1 activity and reduced gene dosage of *PTEN*, which were recently shown to be of great importance for repair of CPT-induced DNA damage.

CPT-resistant cell lines have variable degrees of resistance to CPT and variable dependency on the presence of CPT to retain their resistance to it. These observations may relate to mechanisms implicated in their resistance. Only a few CPT-resistant cell lines have been examined at the genomic level, and clearly, more CPT-resistant cell lines need to be examined with up-to-date genomic methods in order to enhance the understanding of their resistance mechanisms. Furthermore, it should be kept in mind that CPT-resistant cell lines are developed by exposure to longitudinal increments of sublethal drug doses, and often prior to their selection, had a mutagenic step, which may provide the cells with potential initial genomic aberrations amenable to selective advantage. This is different to the clinical situation in that patients becoming resistant to treatment with CPT-derived drugs did not have an initial mutagenic step and most often no increment in drug dose.

Nevertheless, identification of recurrent regions implicated in the acquisition of CPT resistance might provide the first clues to identifying important regions of the genome, and consequently genes, which could serve as potential therapeutic targets for intervention against development of CPT resistance, or for its reversal.

Conflicts of Interest

The Authors declare no conflicts of interest in regard to this study.

Acknowledgements

The biotechnologists Bente Madsen and Pia Kristensen are greatly thanked for excellent technical assistance. Technician Noriko Hansen is thanked for purification of human TOP1. Dr. Christopher Veigaard is greatly thanked for providing cell growth characteristics. The Danish Cancer Society supported the study.

References

1 Kantarjian HM, Beran M, Ellis A, Zwelling L, O'Brien S, Cazenave L, Koller C, Rios MB, Plunkett W and Keating MJ: Phase I study of Topotecan, a new topoisomerase I inhibitor, in patients with refractory or relapsed acute leukemia. Blood *81*: 1146-1151, 1993.

2 Smith DH, Adams JR, Johnston SR, Gordon A, Drummond MF and Bennett CL: A comparative economic analysis of pegylated liposomal doxorubicin *versus* topotecan in ovarian cancer in the USA and the UK. Ann Oncol *13*: 1590-1597, 2002.

3 Tsavaris N, Kosmas C, Skopelitis H, Papadoniou N, Polyzos A, Zografos G, Adoniou E, Gryniatsos J, Felekouras E, Zacharakis M, Sigala F, Bacoyiannis C, Papastratis G and Papalambros E: Sequential administration of 5-fluorouracil (5FU)/leucovorin (LV) followed by irinotecan (CPT-11) at relapse *versus* CPT-11 followed by 5-FU/LV in advanced colorectal carcinoma. A phase III randomized study. Chemotherapy *53*: 282-291, 2007.

4 Riemsma R, Simons JP, Bashir Z, Gooch CL and Kleijnen J: Systematic Review of topotecan (Hycamtin) in relapsed small cell lung cancer. BMC Cancer *10*: 436, 2010.

5 Douillard JY, Cunningham D, Roth AD, Navarro M, James RD, Karasek P, Jandik P, Iveson T, Carmichael J, Alakl M, Gruia G, Awad L and Rougier P: Irinotecan combined with fluorouracil

compared with fluorouracil alone as first-line treatment for metastatic colorectal cancer: a multicentre randomised trial. Lancet *355*: 1041-1047, 2000.
6 Beretta GL, Gatti L, Perego P and Zaffaroni N: Camptothecin resistance in cancer: insights into the molecular mechanisms of a DNA-damaging drug. Curr Med Chem *20*: 1541-1565, 2013.
7 Pommier Y: Topoisomerase I inhibitors: camptothecins and beyond. Nat Rev Cancer *6*: 789-802, 2006.
8 Wang JC: Cellular roles of DNA topoisomerases: a molecular perspective. Nat Rev Mol Cell Biol *3*: 430-440, 2002.
9 Rossi F, Labourier E, Forne T, Divita G, Derancourt J, Riou JF, Antoine E, Cathala G, Brunel C and Tazi J: Specific phosphorylation of SR proteins by mammalian DNA topoisomerase I. Nature *381*: 80-82, 1996.
10 Pfister TD, Reinhold WC, Agama K, Gupta S, Khin SA, Kinders RJ, Parchment RE, Tomaszewski JE, Doroshow JH and Pommier Y: Topoisomerase I levels in the NCI-60 cancer cell line panel determined by validated ELISA and microarray analysis and correlation with indenoisoquinoline sensitivity. Mol Cancer Ther *8*: 1878-1884, 2009.
11 Andoh T, Ishii K, Suzuki Y, Ikegami Y, Kusunoki Y, Takemoto Y and Okada K: Characterization of a mammalian mutant with a camptothecin-resistant DNA topoisomerase I. Proc Natl Acad Sci USA *84*: 5565-5569, 1987.
12 Kanzawa F, Sugimoto Y, Minato K, Kasahara K, Bungo M, Nakagawa K, Fujiwara Y, Liu LF and Saijo N: Establishment of a camptothecin analogue (CPT-11)-resistant cell line of human non-small cell lung cancer: characterization and mechanism of resistance. Cancer Res *50*: 5919-5924, 1990.
13 Kubota N, Kanzawa F, Nishio K, Takeda Y, Ohmori T, Fujiwara Y, Terashima Y and Saijo N: Detection of topoisomerase I gene point mutation in CPT-11 resistant lung cancer cell line. Biochem Biophys Res Commun *188*: 571-577, 1992.
14 Sugimoto Y, Tsukahara S, Oh-hara T, Isoe T and Tsuruo T: Decreased expression of DNA topoisomerase I in camptothecin-resistant tumor cell lines as determined by a monoclonal antibody. Cancer Res *50*: 6925-6930, 1990.
15 Rubin E, Pantazis P, Bharti A, Toppmeyer D, Giovanella B and Kufe D: Identification of a mutant human topoisomerase I with intact catalytic activity and resistance to 9-nitro-camptothecin. J Biol Chem *269*: 2433-2439, 1994.
16 Fujimori A, Harker WG, Kohlhagen G, Hoki Y and Pommier Y: Mutation at the catalytic site of topoisomerase I in CEM/C2, a human leukemia cell line resistant to camptothecin. Cancer Res *55*: 1339-1346, 1995.
17 Chatterjee D, Wyche JH and Pantazis P: Induction of apoptosis in malignant and camptothecin-resistant human cells. Ann N Y Acad Sci *803*: 143-156, 1996.
18 Urasaki Y, Laco GS, Pourquier P, Takebayashi Y, Kohlhagen G, Gioffre C, Zhang H, Chatterjee D, Pantazis P and Pommier Y: Characterization of a novel topoisomerase I mutation from a camptothecin-resistant human prostate cancer cell line. Cancer Res *61*: 1964-1969, 2001.
19 Saleem A, Ibrahim N, Patel M, Li XG, Gupta E, Mendoza J, Pantazis P and Rubin EH: Mechanisms of resistance in a human cell line exposed to sequential topoisomerase poisoning. Cancer Res *57*: 5100-5106, 1997.
20 Chang JY, Liu JF, Juang SH, Liu TW and Chen LT: Novel mutation of topoisomerase I in rendering cells resistant to camptothecin. Cancer Res *62*: 3716-3721, 2002.
21 Gao K, Lockwood WW, Li J, Lam W and Li G: Genomic analyses identify gene candidates for acquired irinotecan resistance in melanoma cells. Int J Oncol *32*: 1343-1349, 2008.
22 Petitprez A, Poindessous V, Ouaret D, Regairaz M, Bastian G, Guerin E, Escargueil AE and Larsen AK: Acquired irinotecan resistance is accompanied by stable modifications of cell cycle dynamics independent of MSI status. Int J Oncol *42*: 1644-1653, 2013.
23 Tuduri S, Crabbe L, Conti C, Tourriere H, Holtgreve-Grez H, Jauch A, Pantesco V, De Vos J, Thomas A, Theillet C, Pommier Y, Tazi J, Coquelle A and Pasero P: Topoisomerase I suppresses genomic instability by preventing interference between replication and transcription. Nat Cell Biol *11*: 1315-1324, 2009.
24 Kjeldsen E, Bonven BJ andoh T, Ishii K, Okada K, Bolund L and Westergaard O: Characterization of a camptothecin-resistant human DNA topoisomerase I. J Biol Chem *263*: 3912-3916, 1988.
25 Roy A, Tesauro C, Frohlich R, Hede MS, Nielsen MJ, Kjeldsen E, Bonven B, Stougaard M, Gromova I and Knudsen BR: Decreased camptothecin sensitivity of the stem-cell-like fraction of Caco2 cells correlates with an altered phosphorylation pattern of topoisomerase I. PloS One *9*: e99628, 2014.
26 Jensen PW, Falconi M, Kristoffersen EL, Simonsen AT, Cifuentes JB, Marcussen LB, Frohlich R, Vagner J, Harmsen C, Juul S, Ho YP, Withers MA, Lupski JR, Koch J, Desideri A, Knudsen BR and Stougaard M: Real-time detection of TDP1 activity using a fluorophore-quencher coupled DNA-biosensor. Biosens Bioelectron *48*: 230-237, 2013.
27 Lisby M, Krogh BO, Boege F, Westergaard O and Knudsen BR: Camptothecins inhibit the utilization of hydrogen peroxide in the ligation step of topoisomerase I catalysis. Biochemistry *37*: 10815-10827, 1998.
28 Veigaard C and Kjeldsen E: Exploring the genome-wide relation between copy number status and microRNA expression. Genomics *104*: 271-278, 2014.
29 ISCN: An International System for Human Cytogenetic Nomenclature (2013). Shaffer LG, McGowan-Jordan and Schmid M (Eds.) Basel: S. Karger and Cytogenetic and Genome Research, 2013.
30 Kerndrup GB and Kjeldsen E: Acute leukemia cytogenetics: an evaluation of combining G-band karyotyping with multi-color spectral karyotyping. Cancer Genet Cytogenet *124*: 7-11, 2001.
31 Kjeldsen E and Roug AS: A novel unbalanced *de novo* translocation der(5)t(4;5)(q26;q21.1) in adult T-cell precursor lymphoblastic leukemia. Mol Cytogenet *5*: 21, 2012.
32 Braylan RC, Orfao A, Borowitz MJ and Davis BH: Optimal number of reagents required to evaluate hematolymphoid neoplasias: results of an international consensus meeting. Cytometry *46*: 23-27, 2001.
33 Christiansen K, Svejstrup AB andersen AH and Westergaard O: Eukaryotic topoisomerase I-mediated cleavage requires bipartite DNA interaction. Cleavage of DNA substrates containing strand interruptions implicates a role for topoisomerase I in illegitimate recombination. J Biol Chem *268*: 9690-9701, 1993.
34 Tamura H, Kohchi C, Yamada R, Ikeda T, Koiwai O, Patterson E, Keene JD, Okada K, Kjeldsen E, Nishikawa K and Andoh T: Molecular cloning of a cDNA of a camptothecin-resistant human DNA topoisomerase I and identification of mutation sites. Nucleic Acids Res *19*: 69-75, 1991.

35 Stougaard M, Lohmann JS, Mancino A, Celik S, Andersen FF, Koch J and Knudsen BR: Single-molecule detection of human topoisomerase I cleavage-ligation activity. ACS Nano *3*: 223-233, 2009.

36 Andersen FF, Stougaard M, Jorgensen HL, Bendsen S, Juul S, Hald K andersen AH, Koch J and Knudsen BR: Multiplexed detection of site specific recombinase and DNA topoisomerase activities at the single molecule level. ACS Nano *3*: 4043-4054, 2009.

37 Huang CC, Hou Y, Woods LK, Moore GE and Minowada J: Cytogenetic study of human lymphoid T-cell lines derived from lymphocytic leukemia. J Natl Cancer Inst *53*: 655-660, 1974.

38 Hayata I, Oshimura M, Minowada J and Sandberg AA: Chromosomal banding of cultured T and B lymphocytes. In Vitro *11*: 361-368, 1975.

39 Le Beau MM, McKeithan TW, Shima EA, Goldman-Leikin RE, Chan SJ, Bell GI, Rowley JD and Diaz MO: T-cell receptor alpha-chain gene is split in a human T-cell leukemia cell line with a t(11;14)(p15;q11). Proc Natl Acad Sci USA *83*: 9744-9748, 1986.

40 McGuire EA, Hockett RD, Pollock KM, Bartholdi MF, O'Brien SJ and Korsmeyer SJ: The t(11;14)(p15;q11) in a T-cell acute lymphoblastic leukemia cell line activates multiple transcripts, including Ttg-1, a gene encoding a potential zinc finger protein. Mol Cell Biol *9*: 2124-2132, 1989.

41 Kjeldsen E, Tordrup D, Hubner GM, Knudsen BR and Andersen FF: Topoisomerase I deficiency results in chromosomal alterations in cervical cancer cells. Anticancer Res *30*: 3257-3265, 2010.

42 Salido M, Arriola E, Carracedo A, Canadas I, Rovira A, Espinet B, Rojo F, Arumi M, Serrano S, Albanell J and Sole F: Cytogenetic characterization of NCI-H69 and NCI-H69AR small cell lung cancer cell lines by spectral karyotyping. Cancer Genet Cytogenet *191*: 97-101, 2009.

43 Rao VK, Wangsa D, Robey RW, Huff L, Honjo Y, Hung J, Knutsen T, Ried T and Bates SE: Characterization of ABCG2 gene amplification manifesting as extrachromosomal DNA in mitoxantrone-selected SF295 human glioblastoma cells. Cancer Genet Cytogenet *160*: 126-133, 2005.

44 Yasui K, Mihara S, Zhao C, Okamoto H, Saito-Ohara F, Tomida A, Funato T, Yokomizo A, Naito S, Imoto I, Tsuruo T and Inazawa J: Alteration in copy numbers of genes as a mechanism for acquired drug resistance. Cancer Res *64*: 1403-1410, 2004.

45 Veigaard C and Kjeldsen E: microRNA global expression analysis and genomic profiling of the camptothecin-resistant T-ALL derived cell line CPT-K5. RNA Dis *1*: 12, 2014.

46 Przybytkowski E, Lenkiewicz E, Barrett MT, Klein K, Nabavi S, Greenwood CM and Basik M: Chromosome-breakage genomic instability and chromothripsis in breast cancer. BMC Genomics *15*: 579, 2014.

47 Jones MJ and Jallepalli PV: Chromothripsis: chromosomes in crisis. Dev Cell *23*: 908-917, 2012.

48 Kloosterman WP, Hoogstraat M, Paling O, Tavakoli-Yaraki M, Renkens I, Vermaat JS, van Roosmalen MJ, van Lieshout S, Nijman IJ, Roessingh W, van 't Slot R, van de Belt J, Guryev V, Koudijs M, Voest E and Cuppen E: Chromothripsis is a common mechanism driving genomic rearrangements in primary and metastatic colorectal cancer. Genome Biol *12*: R103, 2011.

49 Lapuk AV, Wu C, Wyatt AW, McPherson A, McConeghy BJ, Brahmbhatt S, Mo F, Zoubeidi A anderson S, Bell RH, Haegert A, Shukin R, Wang Y, Fazli L, Hurtado-Coll A, Jones EC, Hach F, Hormozdiari F, Hajirasouliha I, Boutros PC, Bristow RG, Zhao Y, Marra MA, Fanjul A, Maher CA, Chinnaiyan AM, Rubin MA, Beltran H, Sahinalp SC, Gleave ME, Volik SV and Collins CC: From sequence to molecular pathology and a mechanism driving the neuroendocrine phenotype in prostate cancer. J Pathol *227*: 286-297, 2012.

50 Magrangeas F, Avet-Loiseau H, Munshi NC and Minvielle S: Chromothripsis identifies a rare and aggressive entity among newly diagnosed multiple myeloma patients. Blood *118*: 675-678, 2011.

51 Molenaar JJ, Koster J, Zwijnenburg DA, van Sluis P, Valentijn LJ, van der Ploeg I, Hamdi M, van Nes J, Westerman BA, van Arkel J, Ebus ME, Haneveld F, Lakeman A, Schild L, Molenaar P, Stroeken P, van Noesel MM, Ora I, Santo EE, Caron HN, Westerhout EM and Versteeg R: Sequencing of neuroblastoma identifies chromothripsis and defects in neuritogenesis genes. Nature *483*: 589-593, 2012.

52 Rausch T, Jones DT, Zapatka M, Stutz AM, Zichner T, Weischenfeldt J, Jager N, Remke M, Shih D, Northcott PA, Pfaff E, Tica J, Wang Q, Massimi L, Witt H, Bender S, Pleier S, Cin H, Hawkins C, Beck C, von Deimling A, Hans V, Brors B, Eils R, Scheurlen W, Blake J, Benes V, Kulozik AE, Witt O, Martin D, Zhang C, Porat R, Merino DM, Wasserman J, Jabado N, Fontebasso A, Bullinger L, Rucker FG, Dohner K, Dohner H, Koster J, Molenaar JJ, Versteeg R, Kool M, Tabori U, Malkin D, Korshunov A, Taylor MD, Lichter P, Pfister SM and Korbel JO: Genome sequencing of pediatric medulloblastoma links catastrophic DNA rearrangements with TP53 mutations. Cell *148*: 59-71, 2012.

53 Rasheed ZA and Rubin EH: Mechanisms of resistance to topoisomerase I-targeting drugs. Oncogene *22*: 7296-7304, 2003.

54 Rubin EH, Li TK, Duann P and Liu LF: Cellular resistance to topoisomerase poisons. Cancer Treat and Res *87*: 243-260, 1996.

55 Liao Z, Robey RW, Guirouilh-Barbat J, To KK, Polgar O, Bates SE and Pommier Y: Reduced expression of DNA topoisomerase I in SF295 human glioblastoma cells selected for resistance to homocamptothecin and diflomotecan. Mol Pharmacol *73*: 490-497, 2008.

56 Pommier Y, Pourquier P, Urasaki Y, Wu J and Laco GS: Topoisomerase I inhibitors: selectivity and cellular resistance. Drug Resist Updat *2*: 307-318, 1999.

57 Chrencik JE, Staker BL, Burgin AB, Pourquier P, Pommier Y, Stewart L and Redinbo MR: Mechanisms of camptothecin resistance by human topoisomerase I mutations. J Mol Biol *339*: 773-784, 2004.

58 Mo W and Zhang JT: Human ABCG2: structure, function and its role in multidrug resistance. Int J Biochem Mol Biol *3*: 1-27, 2012.

59 Hoki Y, Fujimori A and Pommier Y: Differential cytotoxicity of clinically important camptothecin derivatives in P-glycoprotein-overexpressing cell lines. Cancer Chemother Pharmacol *40*: 433-438, 1997.

60 Brangi M, Litman T, Ciotti M, Nishiyama K, Kohlhagen G, Takimoto C, Robey R, Pommier Y, Fojo T and Bates SE: Camptothecin resistance: role of the ATP-binding cassette (ABC), mitoxantrone-resistance half-transporter (MXR) and potential for glucuronidation in MXR-expressing cells. Cancer Res *59*: 5938-5946, 1999.

61 Rajendra R, Gounder MK, Saleem A, Schellens JH, Ross DD, Bates SE, Sinko P and Rubin EH: Differential effects of the breast cancer resistance protein on the cellular accumulation and cytotoxicity of 9-aminocamptothecin and 9-nitrocamptothecin. Cancer Res *63*: 3228-3233, 2003.

62 Ross DD, Yang W, Abruzzo LV, Dalton WS, Schneider E, Lage H, Dietel M, Greenberger L, Cole SP and Doyle LA: Atypical multidrug resistance: breast cancer resistance protein messenger RNA expression in mitoxantrone-selected cell lines. J Natl Cancer Inst *91*: 429-433, 1999.

63 Candeil L, Gourdier I, Peyron D, Vezzio N, Copois V, Bibeau F, Orsetti B, Scheffer GL, Ychou M, Khan QA, Pommier Y, Pau B, Martineau P and Del Rio M: ABCG2 overexpression in colon cancer cells resistant to SN38 and in irinotecan-treated metastases. Int J Cancer *109*: 848-854, 2004.

64 Su Y, Lee SH and Sinko PJ: Inhibition of efflux transporter ABCG2/BCRP does not restore mitoxantrone sensitivity in irinotecan-selected human leukemia CPT-K5 cells: evidence for multifactorial multidrug resistance. Eur J Pharm Sci *29*: 102-110, 2006.

65 Bates SE, Medina-Perez WY, Kohlhagen G, Antony S, Nadjem T, Robey RW and Pommier Y: ABCG2 mediates differential resistance to SN-38 (7-ethyl-10-hydroxycamptothecin) and homocamptothecins. J Pharmacol Exp Ther *310*: 836-842, 2004.

66 Maliepaard M, van Gastelen MA, de Jong LA, Pluim D, van Waardenburg RC, Ruevekamp-Helmers MC, Floot BG and Schellens JH: Overexpression of the BCRP/MXR/ABCP gene in a topotecan-selected ovarian tumor cell line. Cancer Res *59*: 4559-4563, 1999.

67 Kawabata S, Oka M, Shiozawa K, Tsukamoto K, Nakatomi K, Soda H, Fukuda M, Ikegami Y, Sugahara K, Yamada Y, Kamihira S, Doyle LA, Ross DD and Kohno S: Breast cancer resistance protein directly confers SN-38 resistance of lung cancer cells. Biochem Biophys Res Commun *280*: 1216-1223, 2001.

68 Tomicic MT and Kaina B: Topoisomerase degradation, DSB repair, p53 and IAPs in cancer cell resistance to camptothecin-like topoisomerase I inhibitors. Biochim Biophys Acta *1835*: 11-27, 2013.

69 Nieves-Neira W and Pommier Y: Apoptotic response to camptothecin and 7-hydroxystaurosporine (UCN-01) in the 8 human breast cancer cell lines of the NCI Anticancer Drug Screen: multifactorial relationships with topoisomerase I, protein kinase C, Bcl-2, p53, MDM-2 and caspase pathways. Int J Cancer *82*: 396-404, 1999.

70 Roos WP and Kaina B: DNA damage-induced cell death by apoptosis. Trends Mol Med *12*: 440-450, 2006.

71 Dubrez L, Goldwasser F, Genne P, Pommier Y and Solary E: The role of cell cycle regulation and apoptosis triggering in determining the sensitivity of leukemic cells to topoisomerase I and II inhibitors. Leukemia *9*: 1013-1024, 1995.

72 Solary E, Dubrez L, Eymin B, Bertrand R and Pommier Y: Apoptosis of human leukemic cells induced by topoisomerase I and II inhibitors. Bull Cancer *83*: 205-212, 1996.

73 Beretta GL, Perego P and Zunino F: Targeting topoisomerase I: molecular mechanisms and cellular determinants of response to topoisomerase I inhibitors. Expert Opin Ther Targets *12*: 1243-1256, 2008.

74 Pommier Y, Huang SY, Gao R, Das BB, Murai J and Marchand C: Tyrosyl-DNA-phosphodiesterases (TDP1 and TDP2). DNA Repair (Amst) *19*: 114-129, 2014.

75 Desai SD, Liu LF, Vazquez-Abad D and D'Arpa P: Ubiquitin-dependent destruction of topoisomerase I is stimulated by the antitumor drug camptothecin. J Biol Chem *272*: 24159-24164, 1997.

76 Takahata C, Masuda Y, Takedachi A, Tanaka K, Iwai S and Kuraoka I: Repair synthesis step involving ERCC1-XPF participates in DNA repair of the Top1-DNA damage complex. Carcinogenesis *36*: 841-851, 2015.

77 Takashima H, Boerkoel CF, John J, Saifi GM, Salih MA, Armstrong D, Mao Y, Quiocho FA, Roa BB, Nakagawa M, Stockton DW and Lupski JR: Mutation of TDP1, encoding a topoisomerase I-dependent DNA damage repair enzyme, in spinocerebellar ataxia with axonal neuropathy. Nat Genet *32*: 267-272, 2002.

78 Das BB, Huang SY, Murai J, Rehman I, Ame JC, Sengupta S, Das SK, Majumdar P, Zhang H, Biard D, Majumder HK, Schreiber V and Pommier Y: PARP1-TDP1 coupling for the repair of topoisomerase I-induced DNA damage. Nucleic Acids Res *42*: 4435-4449, 2014.

79 Ando K, Shah AK, Sachdev V, Kleinstiver BP, Taylor-Parker J, Welch MM, Hu Y, Salgia R, White FM, Parvin JD, Ozonoff A, Rameh LE, Joung JK and Bharti AK: Camptothecin resistance is determined by the regulation of topoisomerase I degradation mediated by ubiquitin proteasome pathway. Oncotarget *8*: 43733-43751, 2017.

80 Yamauchi T, Yoshida A and Ueda T: Camptothecin induces DNA strand breaks and is cytotoxic in stimulated normal lymphocytes. Oncol Rep *25*: 347-352, 2011.

81 Sakofsky CJ, Ayyar S and Malkova A: Break-induced replication and genome stability. Biomolecules *2*: 483-504, 2012.

82 Leffak M: Break-induced replication links microsatellite expansion to complex genome rearrangements. Bioessays *39(8)*: 2017. doi: 10.1002/bies.201700025.

83 Hastings PJ, Ira G and Lupski JR: A microhomology-mediated break-induced replication model for the origin of human copy number variation. PLoS Genet *5*: e1000327, 2009.

84 Reyes GX, Schmidt TT, Kolodner RD and Hombauer H: New insights into the mechanism of DNA mismatch repair. Chromosoma *124*: 443-462, 2015.

85 Li GM: Mechanisms and functions of DNA mismatch repair. Cell Res *18*: 85-98, 2008.

86 Gomes-Pereira M, Fortune MT, Ingram L, McAbney JP and Monckton DG: Pms2 is a genetic enhancer of trinucleotide CAG.CTG repeat somatic mosaicism: implications for the mechanism of triplet repeat expansion. Hum Mol Genet *13*: 1815-1825, 2004.

87 Pichierri P, Franchitto A, Piergentili R, Colussi C and Palitti F: Hypersensitivity to camptothecin in MSH2 deficient cells is correlated with a role for MSH2 protein in recombinational repair. Carcinogenesis *22*: 1781-1787, 2001.

88 Xiao Z, Chen Z, Gunasekera AH, Sowin TJ, Rosenberg SH, Fesik S and Zhang H: Chk1 mediates S and G2 arrests through Cdc25A degradation in response to DNA-damaging agents. J Biol Chem *278*: 21767-21773, 2003.

89 Nims RW, Sykes G, Cottrill K, Ikonomi P and Elmore E: Short tandem repeat profiling: part of an overall strategy for reducing the frequency of cell misidentification. In Vitro Cell Dev Biol Anim *46*: 811-819, 2010.

90 Kerrigan L and Nims RW: Authentication of human cell-based products: the role of a new consensus standard. Regen Med *6*: 255-260, 2011.
91 Butler JM: Genetics and genomics of core short tandem repeat loci used in human identity testing. J Forensic Sci *51*: 253-265, 2006.
92 Hubert L, Jr., Lin Y, Dion V and Wilson JH: Topoisomerase 1 and single-strand break repair modulate transcription-induced CAG repeat contraction in human cells. Mol Cell Biol *31*: 3105-3112, 2011.
93 Lin Y and Wilson JH: Diverse effects of individual mismatch repair components on transcription-induced CAG repeat instability in human cells. DNA Repair (Amst) *8*: 878-885, 2009.
94 Lin Y and Wilson JH: Transcription-induced CAG repeat contraction in human cells is mediated in part by transcription-coupled nucleotide excision repair. Mol Cell Biol *27*: 6209-6217, 2007.
95 Kim JC and Mirkin SM: The balancing act of DNA repeat expansions. Curr Opin Genet Dev *23*: 280-288, 2013.
96 Yang Z, Lau R, Marcadier JL, Chitayat D and Pearson CE: Replication inhibitors modulate instability of an expanded trinucleotide repeat at the myotonic dystrophy type 1 disease locus in human cells. Am J Hum Genet *73*: 1092-1105, 2003.
97 Park SY, Choi HC, Chun YH, Kim H and Park SH: Characterization of chromosomal aberrations in lung cancer cell lines by cross-species color banding. Cancer Genet Cytogenet *124*: 62-70, 2001.
98 Shipley JM, Sheppard DM and Sheer D: Karyotypic analysis of the human monoblastic cell line U937. Cancer Genet Cytogenet *30*: 277-284, 1988.
99 Pittman SM, Kavallaris M and Stewart BW: Karyotypic analysis of CCRF-CEM and drug-resistant cell lines with stable and unstable ploidy. Cancer Genet Cytogenet *66*: 54-62, 1993.
100 Bernardino J, Bourgeois CA, Muleris M, Dutrillaux AM, Malfoy B and Dutrillaux B: Characterization of chromosome changes in two human prostatic carcinoma cell lines (PC-3 and DU145) using chromosome painting and comparative genomic hybridization. Cancer Genet Cytogenet *96*: 123-128, 1997.
101 Beheshti B, Park PC, Sweet JM, Trachtenberg J, Jewett MA and Squire JA: Evidence of chromosomal instability in prostate cancer determined by spectral karyotyping (SKY) and interphase fish analysis. Neoplasia *3*: 62-69, 2001.

Received November 17, 2017
Revised December 12, 2017
Accepted December 13, 2017